UCLouvain

FACULTE DES SCIENCES

Faculté des sciences

Synthesis and Characterization of Conjugated Sulfonamide Coordination Polymers for Applications in Divalent Ion Cathode Materials

Auteur : Raphaël Delogne

Promoteur: Alexandru Vlad

Lecteurs : Benjamin Elias, Jean-François Gohy, Yann Garcia

Année académique 2022-2023

I. Table of content

II. Acknowledgments

I would like to express my deepest gratitude to Professor Alexandru Vlad for welcoming me into his laboratory and for igniting my interest in energy storage chemistry. His guidance, expertise, and unwavering support throughout this journey have been invaluable. I am truly grateful for the opportunity to work under his supervision.

I would also like to extend my appreciation to Robert Markowski and Tom Goossens for their guidance and assistance during my experiments. Their insightful advice and expertise in the field have been instrumental in shaping my research. I am grateful for their time, patience, and for their careful review of my thesis, which significantly improved its quality.

I would also like to express my recognition to Jérôme Bailly for his careful review of my dissertation and his helpful comments.

Furthermore, I would like to express my sincere gratitude to all the members of NRJ Group. The positive and collaborative work environment provided me with an enriching experience. Their support, encouragement, and fruitful discussions have played a vital role in my growth as a researcher.

I would like to extend my heartfelt appreciation to Professor Benjamin Elias, Professor Jean-François Gohy, and Professor Yann Garcia for their significant role as the evaluators of my thesis.

I would be remiss not to acknowledge the unwavering support of my family, friends and my girlfriend. Their constant encouragement, understanding, and belief in my abilities have been a source of strength throughout this entire journey. I am truly grateful for their love and support.

Finally, I would like to express my appreciation to all those who have contributed, directly or indirectly, to the successful completion of this thesis. Your assistance, encouragement, and presence in my life have been invaluable.

III. Abstract

Global energy consumption heavily relies on fossil fuels, but climate change necessitates sustainable and environmentally friendly electrical energy production. In response to the intermittent nature of renewable energy sources, electrochemical energy storage in batteries has emerged as a promising solution.

Traditional battery materials, predominantly composed of cobalt and lithium, face limitations due to availability and environmental impacts. To address these challenges, interest has been growing in exploring alternative materials based on organic compounds. These organic-based materials offer several advantages, including the abundance of elemental sources, tunability, and stability.

Among these materials, sulfonamide compounds, particularly Li_4-PTtSA, have shown exceptional retention capacity and coulombic efficiency. Incorporating these compounds into coordination polymers provides a solution to the solubility issues typically encountered in other organic materials. Furthermore, the inclusion of zinc in the coordination structure enhances conductivity and voltage.

The primary objective of this research is to investigate the performance of lithium-free coordination polymers synthesized from sulfonamide molecules coordinated with zinc as cathodic materials in electrochemical energy storage devices. Specifically, the study aims at comparing the performances of polymers containing light divalent ions such as calcium and magnesium with samples containing heavier divalent ions like strontium and barium. This comparative analysis will help identifying the specific effects of different divalent ions on the cycling properties of the coordination polymer.

Through comprehensive comparative analysis, this master thesis research purpose to address key questions related to optimal synthesis conditions, suitable carbon additives, and effective electrolyte choices for enhancing battery performances. The findings have the potential to contribute to the development of sustainable and efficient electrochemical energy storage technologies, advancing the transition towards a greener and more sustainable energy future.

IV. Abbreviations

^{1}H-NMR	Proton Nuclear Magnetic Resonance
COF	Covalent Organic Frameworks
CP	Coordination Polymer
CSA	Conjugated Sulfonamides
DEC	Diethyl Carbonate
DME	Dimethoxyethane,
DME	Dimethoxy Ethane
EC	Ethylene Carbonate
EESS	Electrochemical Energy Storage Systems
EMC	Ethyl Methyl Carbonate
EV	Electric Vehicle
EXAFS	Extended X-Ray Absorption Fine Structure
FTIR	Fourier-Transform Infrared Spectroscopy
GITT	Galvanostatic Intermittent Titration Technique
HOMO	Highest Occupied Molecular Orbital
ICP	Inductively Coupled Plasma Emission
KB	Ketjenblack Carbon
KIB	K-Ion Battery
LIB	Lithium-Ion Battery
LMO	Lithium transition Metal Oxides
LUMO	Lowest Unoccupied Molecular Orbital
MIB	Magnesium-Ion Battery
MOF	Metal Organic Framework
NHE	Normal Hydrogen Electrode
NIB	Na-Ion Battery
NMC	$LiNiMnCoO_2$
OBM	Organic Battery Material
PC	Propylene Carbonate
p-PDSA	1,4-phenylenebis((methylsulfonyl)amide
PTFE	Polytetrafluoroethylene
PTtSA	Benzene-1,2,4,5-tetra-methylsulfonamide
PXRD	Powder X-ray Diffraction
SEI	Solid-Electrolyte Interphase
SP	Super P
SPM	Scanning Probe Microscopy
TEM	Transmission Electron Microscopy
TFSI	Trifluoromethanesulfonimide
THF	Tetrahydrofuran
TM	Transition Metals
XANES	X-ray Absorption Near Edge Structure

V. Introduction

1. General Context of Energy Consumption in the World

Mankind has never been better off than now. The industrialisation of the world has led to the development of revolutionary technologies such as telecommunications, fast long-distance transport and heating for every home. The living standard of an average European today is far superior to that of the kings and princes who ruled the continent 1000 years ago. It is estimated that to maintain their standards of living, each would need 500 "energy slaves", which means 500 times the mechanical and thermal energy one person is able to produce in a 24-hour day [1] (Figure 1).

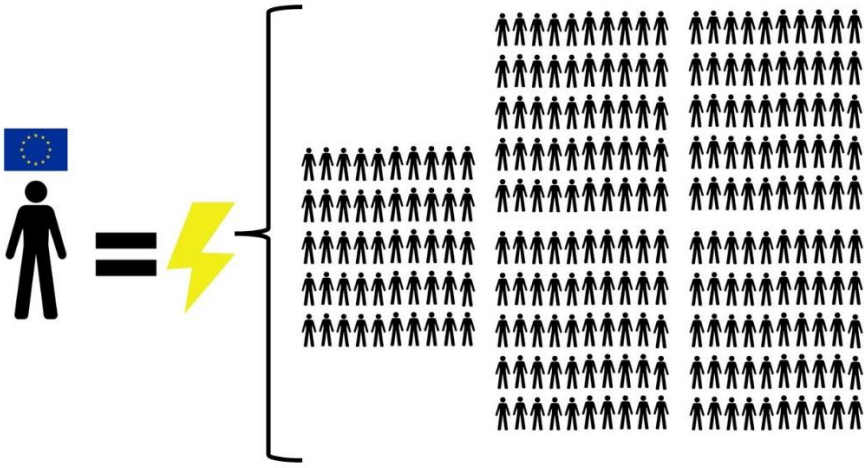

Figure 1: Energy consumption of one average European in "energy slave unit".

Over the past 250 years, our improved and extended lives have been made possible by this energy, primarily derived from fossil fuels. However, the consequential growth in population has resulted in a significant growth in our worldwide energy usage, giving rise to the challenges we presently confront, including climate change and an energy shortage.

Despite the fact that the proportion of renewable energy has never been as high as it is today, the annual growth of global CO_2 emissions has never been that fast [2].

In the context of this climate and energetical crisis we are facing, it is becoming mandatory to produce more energy, notably electrical, in a greener and sustainable way [3]. In order to mitigate the adverse effects of climate change due to greenhouse gas emissions

and to reduce the pressure on the use of finite raw materials like oil and coal, governments around the world are working to develop renewable energy production.

In addition to the environmental arguments, economic and political arguments have motivated investors to increase the budget for renewable energy and fuels in response to the recent Russian aggression on Ukraine. It reached 366 billion USD in 2022, allowing solar and wind energy to provide more than 10% of the world's electricity [4].

The primary challenge associated with generating this renewable energy is its intermittent nature. The sun doesn't shine and the wind doesn't blow always and everywhere at the same power. In consequence the supply of green energy doesn't match the demand (Figure 2). To compensate for this limitation today's scientists are trying to find ways to store it. The idea is to store the excess of energy produced when the demand is low to compensate for the hours when demand is high.

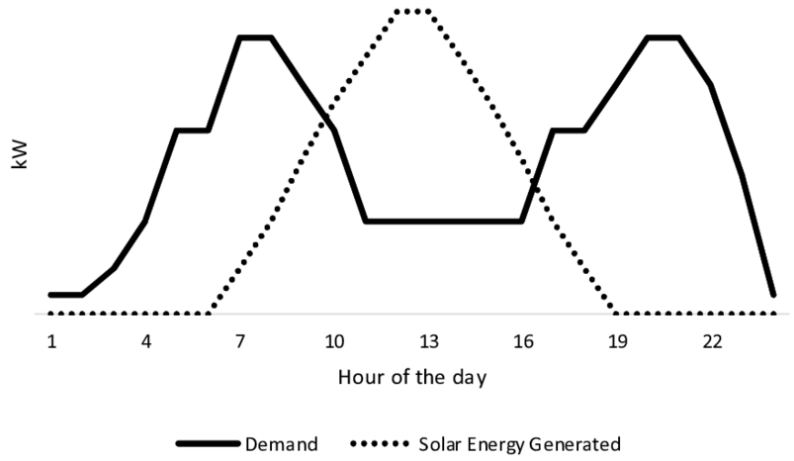

Figure 2: Example of solar energy generation and energy demand during 24 hours, extracted from [5].

Various techniques are commonly employed to store energy, including pumped hydro-power, compressed air, flywheel, and electrochemical storage. These technologies possess distinct performance characteristics, such as their response time to changing demand, the time required to start or stop operations, and their optimal operating points. Among these methods, Electrochemical Energy Storage Systems (EESS) have long been recognized as highly suitable for creating portable energy storage devices. The significance of such systems is especially notable for smartphones, electric vehicles (EVs), and household energy storage, leading to significant global endeavors aimed at enhancing their performance and reducing their environmental impact.

2. Electrochemical Energy Storage System

2.1. Theoretical Concepts

a) Working Mechanism

To understand how we came to make batteries like the one found in our smartphones and in our cars, the first step is to become familiar with their various components and the functioning of the rocking chair mechanism (Figure 3).

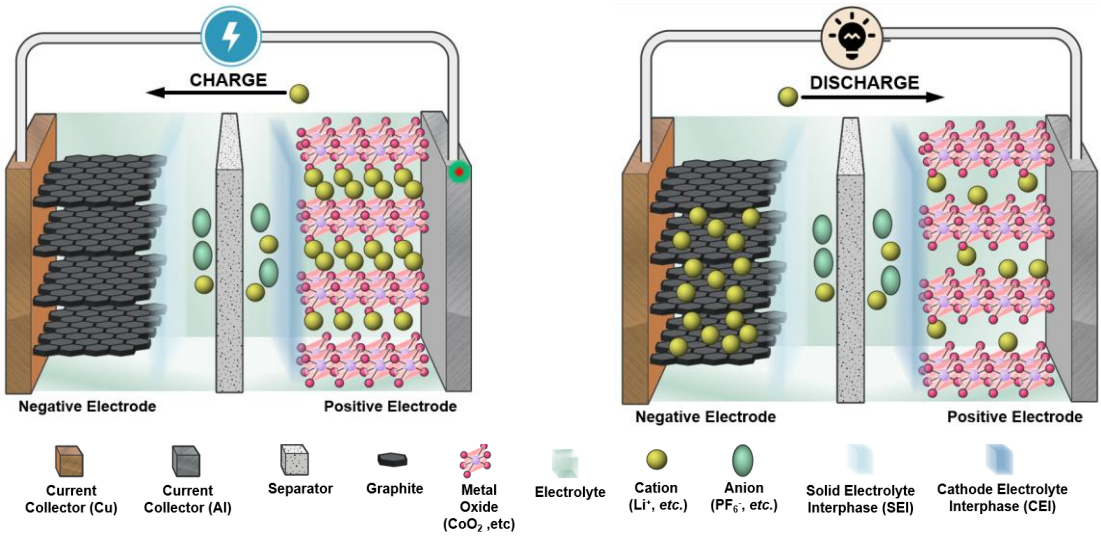

Figure 3: The "rocking chair mechanism" illustrated on a typical modern LIB.

The particularity of batteries compared to other energy storage systems is that the energy is developed through chemical reactions between two electrodes. During the charging process, a voltage is applied forcing a redox reaction to take place. Electrons are transferred from the positive electrode (conventionally called cathode) to the negative electrode (conventionally called anode) through an external wire connecting both electrodes. The charge imbalance induced by the electrons transfer is compensated by the migration of ions from one electrode to the other through the electrolyte, a liquid medium allowing ionic conduction between both sides.

During the discharge, chemical energy is converted into electrical energy via the reverse reaction which takes place spontaneously, creating a reverse current of electrons that can be used to supply a device. The energy associated with this current is determined by the combination of capacity, which refers to the amount of charge transferred, and voltage, which represents the potential difference. Both capacity and voltage are influenced by the specific materials employed.

b) General Parameters

In order for a battery to be considered efficient, it must possess the ability to store a significant amount of chemical energy that can be easily converted into electrical energy. Additionally, it should achieve this while taking up minimal space or weight. To meet these criteria, it is crucial for the positive and negative electrodes to have a low molecular weight and operate at multiple electrons per unit. Furthermore, it is desirable for the potential difference between the two electrodes to be maximized.

The efficiency of a battery is often determined by its energy density. It can be measured in mass units ($Wh.kg^{-1}$) or volume units ($Wh.m^{-3}$) which is respectively the product of the specific or volumetric capacity and capacity and the nominal battery voltage.

The performances of a battery can be studied by galvanic measurements: the cell is charged and discharged in a constant current loop while the voltage evolution is measured. The C-rate measure the rate at which a battery is charged or discharged relative to its capacity. It is calculated by dividing the charging or discharging current by the battery's capacity. For example, a C-rate of 1C means that the charging or discharging current is equal to the battery's nominal capacity. If a battery has a capacity of 1000mAh, a 1C charge rate would be 1000mA (1 ampere). Higher C-rates indicate faster charging or discharging, while lower C-rates indicate slower rates. For instance, a 2C charge rate would charge the same battery in half the time it takes at a 1C rate, while a 0.5C rate would take twice as long.

An additional significant parameter is cycling stability. This parameter, expressed as a percentage, indicates the extent at which the specific capacity of a battery is preserved after consecutive charge and discharge cycles. It can be assessed through two measurements during cycling: capacity retention, obtained through the ratio between discharge capacity of cycle n and first cycle, and columbic efficiency, which quantifies the ratio between the discharge capacity and the charging capacity within the same cycle.

Performance of a battery is not the only parameter that defines its quality (Figure 4). Cost and environmental impact are also to be considered. This can be ensured by modifying the elements involved in the device assembly.

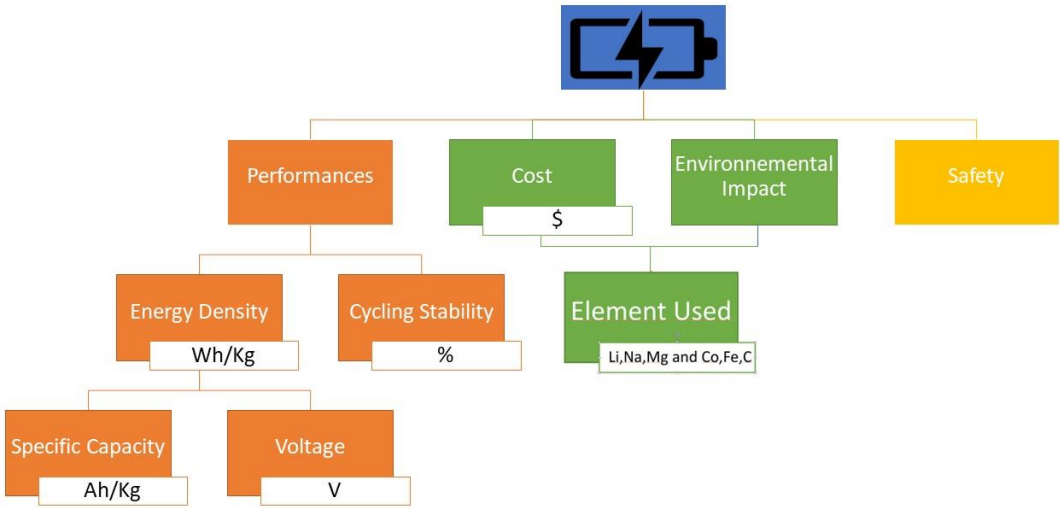

Figure 4: Aspect to consider to fabricate a quality battery.

Finally other parameter to be considered in the batteries is their safety [6] as these can be susceptible of self-ignition and explosion. To avoid this, it is necessary to control the release of heat during use and to avoid short circuits at all costs. The choice of materials and the design of the batteries are also vital. It is necessary to consider the risk of breakage of the protection device and the possibility for the oxygen and water to react with each of the individual components. The Samsung Galaxy Note 7 smartphone serves as a widely recognized illustration of underestimating this parameter, as it necessitated a market recall owing to security issues.

2.2. Lithium-ion Battery: Historical Background and Composition

Lithium is one of the most convenient metal to design batteries thanks to its low molar mass (6.941 $g.mol^{-1}$) and volumetric mass (0.543 $g.cm^{-3}$), which makes it the lightest metal in the periodic table. Additionally, lithium exhibits a theoretical specific capacity of 3860 $Ah.kg^{-1}$ and a standard redox potential of -3.045V vs NHE (Normal Hydrogen Electrode).

As shown on Figure 5 Lithium-ion Batteries (LIBs) currently stand as the optimal choice for electrochemical energy storage due to their superior gravimetric and volumetric energy densities coupled with high voltage range (3-5-4.1 V) and long battery lifespan of up to 2500 cycles[7]. These properties are what make LIB systems so attractive for mobile and compact devices.

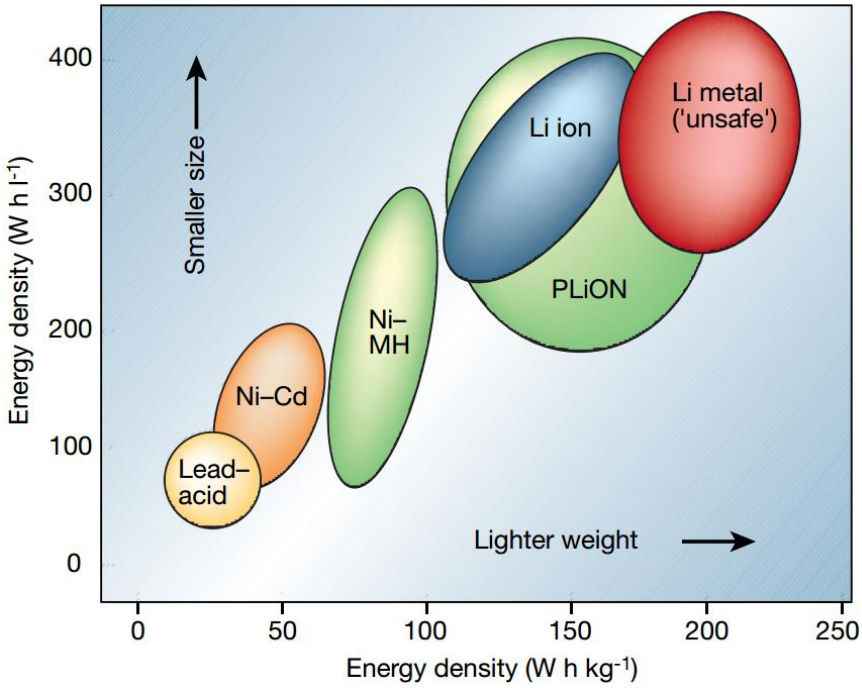

Figure 5: Comparison of the different battery technologies in terms of energy density, extracted from [8].

The advantage of using this metal was first demonstrated in 1970 with the assembly of primary (i.e. not rechargeable) Li cells [9]. During the same period, researchers discovered numerous inorganic compounds that exhibit reversible reactions with alkali metals, including lithium. These discoveries played a crucial role in the advancement of high-energy and sustainable rechargeable systems [10].

In 1972, the American oil and gas company Exxon developed a lithium metal battery with TiS_2 as an intercalation compound for cathode[11,12]. The company published its discovery in the literature, highlighting one of the big problems in rechargeable battery chemistry. During the various charge-discharge cycles of the battery, the lithium was not distributed properly between the two electrodes, which led to the formation of dendrites. This can cause the battery to short-circuit and explode.

It was not until 1980 that Goodenough discovered a series of lithium transition metal oxides (LMO) (ex: $LiCoO_2$, $LiMnO_2$ and $LiNiO_2$) using lithium in its ionic rather than metallic state [13,14]. The advantage of using oxide positive material is twofold. They can phase change to intercalate a large amount of lithium in a reversible manner during the charge/discharge cycles by the rocking chair mechanism and are safe enough to be commercialised.

Regarding the negative electrode of lithium-ion batteries, researchers have explored various types of carbon materials. However, a significant breakthrough occurred when Yasami *et al.* discovered that Li ions could undergo intercalation and deintercalation within the layers of graphite carbon[15].

After a further decade of development, the first lithium-ion battery was released by Sony Corporation [16] . This technology has revolutionised the world, leading to their inventors John B. Goodenough, M. Stanley Whittingham and Akira Yoshino receiving a Nobel Prize in 2019.

The $LiCoO_2$ electrodes can intake and release Li-ions at potentials up to 4.0 V vs. Li^+/Li. The technology has since been optimised to give rise to the so-called "NMC" technology (for $LiNiMnCoO_2$). Even today these layered oxides remain as the favourite cathode materials so far due to their high gravimetric and volumetric energy densities and cyclability [17]. However, its use is limited due to its low abundance and high price[18].

2.3. The future of Lithium and Cobalt in Battery Technology

Lithium is the 32nd most abundant element in the earth's crust. Its quantities are very limited, which makes it one of the elements considered as critical availability. It has a wide range of application in medicine for treatment of manic depression and bipolar disorder [19] and in military for nuclear weapon but it has also g great importance in manufacturing industry with the production of ceramic, glass, lubricants and polymer and in metallurgy (

Figure *6*) [20]. Unsurprisingly, the primary utilization of lithium is battery production, with over 60% of the world's consumption dedicated to this purpose.

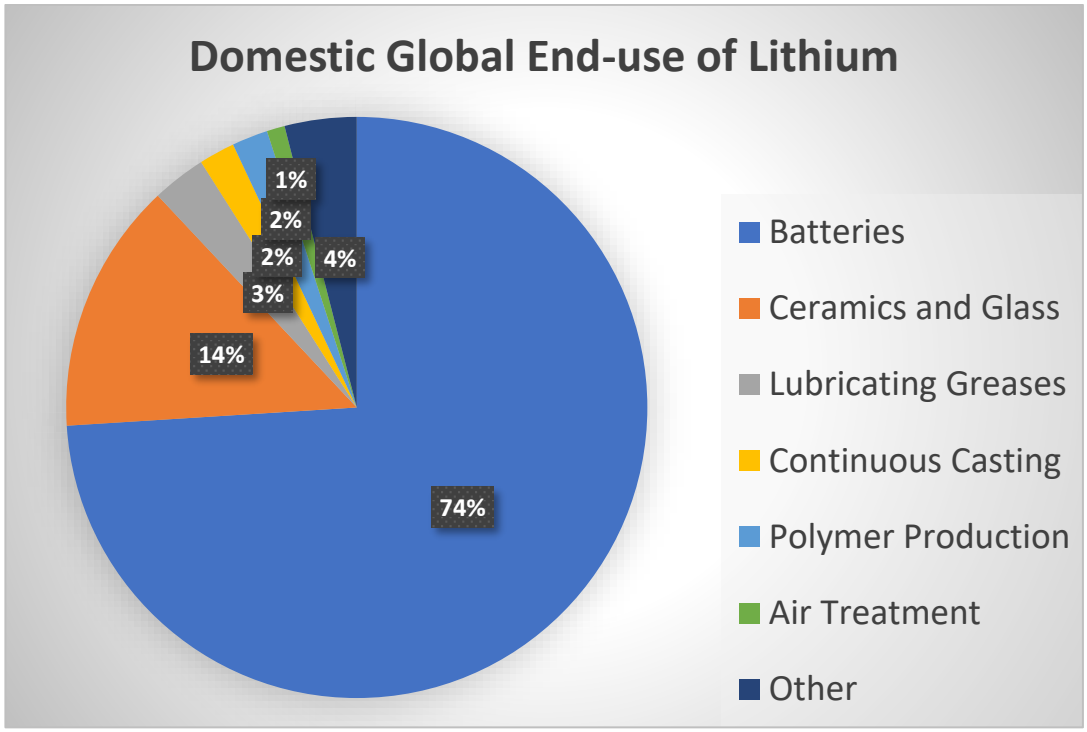

Figure 6: Domestic global end-use of Lithium. Data extracted from [21].

Since the signature of the Kyoto Protocol, Paris Agreement and UN Sustainable Development Goals treaties, the demand for clean and renewable energy production and the energy storage has exploded [20]. These agreements require the use of more low-carbon emission EVs and the development of the renewable energy sector. This growth has caused a significant surge in the pressure to increase the extraction rate of lithium, resulting in a threefold increase over the past decade [20]. Lithium's importance in this context is widely recognized by analysts who often refer to it as "the new white gold", due to its immense value and its limited availability [22].

According to the U.S. Geological Survey Proven global reserves are estimated at 22 Mt (million tonnes) identified resources. It is distributed all over the world but is not economically exploitable everywhere. Argentina, Australia, USA, Chile, Bolivia and China are the most important producers.

With only few suppliers available and the current increase in production demand, one can only expect the prices of any LIB-based device to skyrocket in the coming years [23,24]. Despite the potential to mitigate this growth through the utilization of unconventional lithium sources like seawater and geothermal brines, as well as the development of recycling technologies [20], the projection is that if production continues at the current rate, global lithium reserves are expected to be depleted by 2040 [24]. Similarly, cobalt faces comparable challenges. The quantities of cobalt-containing minerals are limited and will be most likely exhausted within the next 60 years.

Apart from the scarcity of resources, the cobalt extraction raises serious ethical and environmental concerns [25]. Hazardous conditions in the mines of southern Katanga in Congo involve 40.000 children working in dangerous environments without proper safety measures or fair pay according to the estimations. In addition to the human rights issues, cobalt's high toxicity poses health risks that can lead to respiratory disorders, skin irritation, and organ damages [26]. Furthermore, the surrounding ecosystem is also affected, with acid mine drainage contaminating rivers and compromising the safety of drinking water.

In addition to these issues, there are political and economic concerns. Approximately half of the world's cobalt resources are situated in the Democratic Republic of Congo. However, these resources are largely exploited by Chinese industries [27]. Through the Going Out Strategy initiated in 2000, the Chinese government encourages overseas investments, infrastructure projects to extract cobalt in developing nations across Africa and Asia [28]. This monopoly creates limitations on the availability of cobalt for other countries.

Due to its important role in electrification and energy transition, its long-term uncertainties and short-term supply chain bottleneck, cobalt has been classified as a very high criticality risk element by the World Materials Forum [29].

In summary, there exists a significant disparity between the elements required for battery production and their availability on Earth (Figure 7) highlighting an unsustainable long-term situation [8]. It is evident that the development of alternative technologies is imperative to alleviate the strain caused by the extensive utilization of these constituent elements.

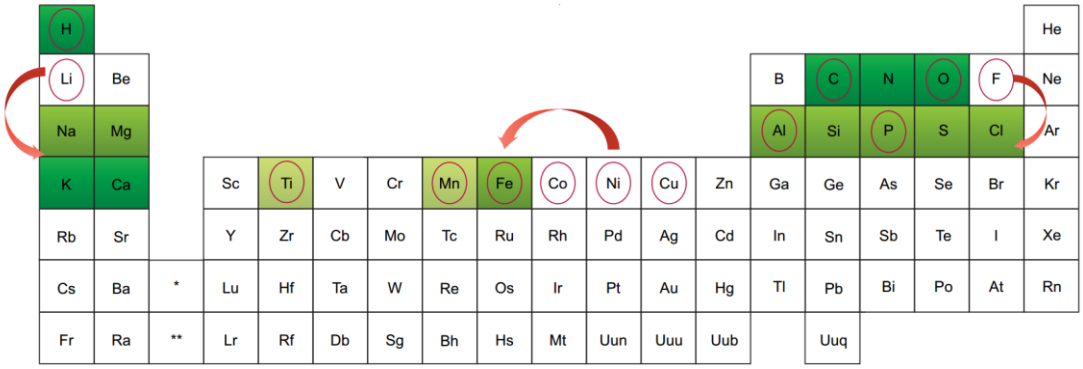

Figure 7: Mismatch between the elements constituting biomass and the main constituents of our present Li-ion batteries. Biomass elements are shown in green (main in dark green, minor in light green, traces in pale green). Present Li-ion batteries main elements are circled in red. The arrows indicate the evolution the battery-constituting elements should follow to better match sustainability issues. Extracted from [8].

In the pursuit of a sustainable future, the need for alternatives to lithium and cobalt becomes evident. "Post-Li technologies" and organic electrode materials serve as viable options, prioritizing safety, environmental friendliness, and economic affordability to facilitate their extensive and enduring adoption. These two concepts will be explored in greater detail in the following sections.

3. Post Li-Technologies

3.1. Sodium and Potassium

Given the rising energy demand and the uncertain future of lithium, it is crucial to develop new battery technologies based on more abundant elements. The post-Li technologies [30], which include battery technologies based on other metals such as Na, K, Mg, Ca, or Zn, present a promising solution. The most common examples of such technologies are Na-Ion batteries (NIBs) and K-ion batteries (KIBs), which have the potential to address the resource challenges associated with traditional LIBs and provide cost-effective alternatives, particularly in applications such as load levelling for power grids where weight and size are less important factors.

For sodium batteries, various cathode materials like layered oxides and polyanionic compounds that are less dependent on Nickel or Cobalt have already exhibited promising performances [30]. Hard carbon remains the only workable anode option for Na-ion systems. The cyclability of these anodes is heavily influenced by the selection of suitable binders and electrolytes. Poor choices in this regard can result in irreversible capacity loss during the initial cycle. This phenomenon is connected to the inferior stability of the solid-electrolyte interphase (SEI) layer when compared to that formed in LIBs.

When it comes to potassium-ion batteries, no cathode materials have been proven to be viable thus far. However, certain polyanionic compounds have shown interesting characteristics such as high voltage and good capacity retention, indicating their potential as cathode materials [31]. On the other hand while graphite can serve as anode for Li-ion batteries, it may no offer sufficient capacity to form practical full cells for K-ion batteries. As result, further efforts are needed to explore alternative anode materials that can provide higher capacity and improve the overall performance of potassium-ion batteries.

3.2. Calcium and Magnesium

Lithium being the lightest element on the periodic table, matching gravimetric energy densities values of materials based on it presents a significant challenge. However, multivalent chemistries offer a interest in volumetric energy density since each multivalent ion carries multiple charges (M^{n+} where n > 1) which results in a greater capacity when storing an equivalent number of active ions within a given volume of electrode compared to monovalent ions.

Moreover, part of their numerous advantages (Figure 8), their abundance and low redox potential (Mg and Ca are −2.37 V and −2.87 V vs SHE respectively) make the use of calcium and magnesium a suitable solution to the lithium crisis.

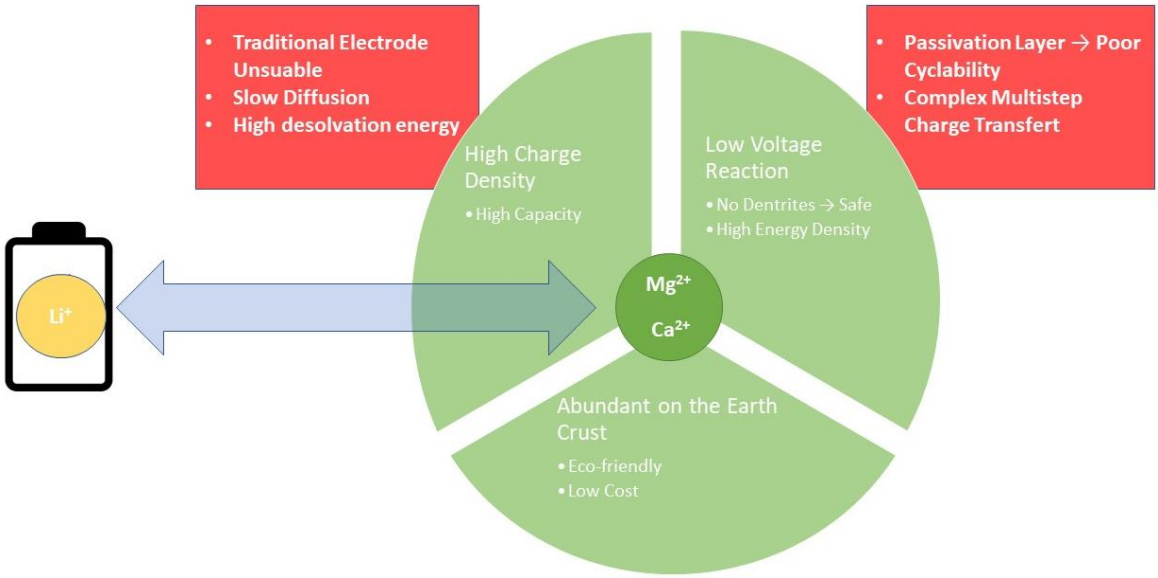

Figure 8: Advantages (green) and drawbacks (red) to replace Li^+ from the batteries by Mg^{2+} or Ca^{2+}.

Compared to Mg, Ca has a lower volumetric and gravimetric capacity, but its redox potential is approximately 0.5 V lower than that of the Mg^{2+}/Mg couple. As a result, Ca has the potential to achieve higher energy density [31].

Moreover, the possibility of employing Mg/Ca-metal as the anode material arises since these metals have a lower propensity to develop dendrites compared to lithium. The occurrence of this phenomenon has been observed in Mg-ion batteries, where the decomposition of the electrolyte leads to the formation of an unevenly distributed ion insulating layer, resulting in localized regions of high current density [32,33].

Generally multivalent metal-ion plating processes result in dense and uniform structures, which help to reduce the specific surface area, minimize the occurrence of secondary reactions [34] and avoid safety issues usually observed for monovalent-ion batteries.

This research field is still at the early stage and further enhancements are required to achieve the same level of performance as that of LIBs. Mg and Ca anodes, non-aqueous liquid organic electrolytes and cathodes still pose challenges that need to be addressed. Indeed, it is not enough to transpose monovalent to polyvalent ion technology to have an efficient battery. To take advantage of their high charge density, the electrodes must be designed to support a similar number of intersection sites but with a higher redox capability. This involves the use of materials and mechanisms that are more complex.

As the energy required to remove the solvent from the metal coordination sphere is substantially higher due to electrostatic forces, the (de)solvation mechanisms need to be very well understood to ensure the reversibility of the process. The redox process happening at the electrodes can occur through various stages, which necessitate an electrolyte that have the capability to endure the decomposition caused by the partially reduced and extremely reactive M^+ metals.

The battery's power is also restricted due to the sluggish movement of divalent ions. These ions have a robust electrostatic interaction with the anion and solvent molecules around them, leading to the formation of a substantial anionic cloud. In the presence of an electric field, this results in retarding forces caused by the relaxation and asymmetry effects, along with the frictional effect caused by the electrophoretic effect. One strategy to overcome this issue is to use large, easily polarisable conter-cations such as sulphides for example.

The kinetic of divalent ions (de)insertion is also slowed by the electrostatic interactions with the cathode materials, which are excessively strong. To expedite the processes at the electrode structures, it is feasible to diminish the migration barriers by reducing the binding energy of the insertion sites and cation. Consequently, unfavourable coordination environments are preferred.

Understanding the behaviour of different solvation structures and the electrochemical behaviour notably the multistep charge-transfer process involved in divalent metal electrodeposition of these ions is the key to improving divalent ion batteries.

a) The Anode Chemistry for Multivalent Metal-ion Batteries

Ongoing research aims to develop anodes and electrolytes that can form an ion permeable solid electrolyte interphase, facilitating ion migration and deposition/strip processes with lower energy requirements. Factors such as temperature and electrolyte concentration impact the feasibility of ion plating by influencing ion pairing tendency, diffusion of M^{n+} ions, desolvation energy, composition and ionic conductivity of the passivation layer. For the moment, research into calcium-ion batteries is still at a very early stage compared with magnesium.

The mechanisms of reaction at the electrodes are diverse (Figure 9). Alloying-type anode materials, with their high specific capacity and excellent cycling performance, are particularly attractive for Mg-ion batteries.

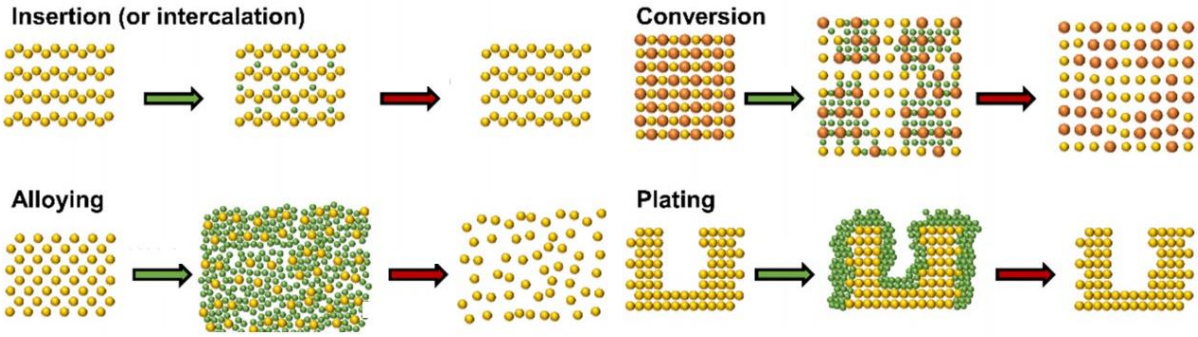

Figure 9: Resume of the working mechanism for anode and cathode materials extracted from [35].

Bismuth-based alloys have shown good reversibility and high theoretical specific capacity (385 $mAh.g^{-1}$), surpassing graphite anodes in lithium-ion batteries [36]. Tin alloys offer advantages such as high theoretical capacity and low volume expansion but face challenges with transport kinetics and reversibility due to sluggish solid-state diffusion and slow interfacial charge transfer [37]. To fully utilize tin alloys, they can be combined with another alloy or used in nanoparticle form [38].

Tin is also used in calcium-ion battery alloys, but their performance is limited under normal conditions [39]. Loss of capacity is often observed between cycles due to instability at the interfaces between the anode and electrolyte [40].

Titanates, such as $Li_4Ti_5O_{12}$, have proven to be suitable anodic materials for Mg-ion batteries (MIBs), offering good reversible capacity and excellent long-term cycle life. Layered $Na_2Ti_3O_7/MgNaTi_3O_7/Mg_{0.5}NaTi_3O_7$ nanoribbons have been described as highly reversible anodes for MIBs [41].

Organic compounds have also been investigated as anodes for calcium batteries but often exhibit stability issues leading to rapid capacity losses. Despite these alternatives, the pure Ca metal anode remains the "holy grail" of calcium-ion batteries [42].

The electrolyte chemistry for multivalent metal-ion batteries also faces challenges when utilizing calcium or magnesium as anodic materials. The main obstacle is the formation of a protective coating during cycling, which hinders ion conduction when in contact with reducible substances in the electrolyte [43,44]. Unlike with lithium, this passivating layer impedes ion flow. Consequently, the selection of electrolytes is limited, and conventional Li-salts such as PF^{6-} or ClO^{4-} are avoided which requires to explore other options [34].

In the early 20th century, Grignard's reagents were used but proved impractical due to low conductivity and stability [45]. Later, a more stable magnesium organo-borate $Mg(BBu_2Ph_2)_2$ in tetrahydrofuran (THF) was preferred [46]. However, its narrow electrochemical window limited its practicality. Other potential like aluminates or bis(trifluoromethane)sulfonimide ($TFSI^-$), have been studied extensively, achieving coulombic efficiencies approaching 100 % [34]. Polar aprotic solvents like alkyl carbonates are suitable for magnesium-ion batteries due to their stability, viscosity, enhanced ionic conductivity, thermal stability and electrochemical stability [47].

Calcium is more reactive than magnesium, leading to the decomposition of anions and electrolytes in ethereal salt solutions. This creates a film on the anode surface, hindering the plating/stripping process and reducing coulombic efficiency [53].

Two approaches have been employed to address compatibility between the electrolyte and calcium anode. One approach involves electrolytes that create a passivation layer on the calcium metal anode, while the other uses electrolytes that are intrinsically stable and do not form a passivation layer, primarily suited for non-metallic anodes [42].

Several electrolytes have been tested, but only a few have shown satisfying performance at room temperature (RT) [47]. Their composition plays a significant role the kinetic and the thermodynamic of calcium plating Recent advancements include using calcium fluoride alkoxyborate in Dimethoxyethane, (DME) solvent, achieving high coulombic efficiencies and anode stability [48].

In addition to conventional salt-in-solvent designs, ionic liquids and solid-state electrolytes composed of ceramics and polymers are being explored [42].

b) The Cathode Chemistry for Multivalent Metal-ion Batteries

Despite what may be assumed, the earliest usage of divalent ion batteries involved the utilization of calcium and not the magnesium. In 1964, these non-rechargeable Ca-batteries were implemented in aeronautics and operated at a high temperature of 450°C[49,50]. Later, other thermal batteries were developed such as Ca-$SOCl_2$. At that time, the issues related to the electrodeposition of metal were not considered a problem because only primary cells were achieved. It was even said to have a safety advantage[51]. However, the development of this technology was not pursued because of the corrosion problems associated with calcium metal[42]. Presently, this problem is addressed through the utilization of electrolytes containing alkyl carbonate at a temperature of 75°, or through the use of $Ca(BH_4)_2$ in THF. In this setup, CaH_2 is generated on the surface of the deposited Ca electrode, preventing any hindrance to the plating and stripping procedure.

In 2000, Aurbach's reported the first prototype rechargeable MIB, which utilized a metal magnesium anode, $Mg(AlCl_2BuEt)_2$ electrolyte, and a Chevrel phase $Mg_xMo_6S_8$ ($0<x<2$) cathode [52]. This system has a theoretical capacity of 129 $mAh.g^{-1}$ at 1.1 V.

Today a multitude of cathode materials exist that can be classified into two main classes, each with their own advantages and drawbacks and their own working mechanisms (Figure 9) [54].

The first and most investigated category for the development of MIBs is still the one which includes the $Mg_xMo_6S_8$: the intercalation compounds. They have the advantage of doing topotactic reactions, where the crystal structures of the reactant and the product are similar. This allows for good cycling stability and fast diffusion of ions through the bulk. It is for these reasons that the LIBs on the market are built with cathodes belonging to this class. Furthermore, the ions' mobility and chemical reaction kinetics of ions within the substance are dependent on various factors such as the connectivity between intercalation sites, channel and cavity widths of the material, and the intercalant and host structure's bond strength.

On the other hand, reversible insertion processes in crystalline compounds can face several challenges. The requirement for high redox potential to enable high cell voltages limits suitable host materials to compounds containing transition metals (TM). The intercalation voltage depends on the nature and oxidation state of the transition-metal ion, as well as the ionocovalent character of the cation-anion bond, primarily driven by the anion's nature and to a lesser extent, the crystal structure. To achieve practical capacities according to theoretical expectations, the crystal and electronic structures must remain stable within the compositional limits of the intercalation reaction. Severe structural rearrangements can be a significant concern, and irreversible structural phase transformations can threaten reversible specific capacity, even if they occur at the microstructure level.

Since their discovery, the Chevrel phase has been optimised to extract large amounts of Mg from its structure. The most successful to date is the one with the formula $Mg_xMo_6S_6Se_2$ with an initial capacity of 110 $mAh.g^{-1}$ at 1.1 V vs Mg/Mg^{2+} in 0.25 M $Mg(AlCl_2BuEt)_2$/THF as the electrolyte [55]. Attempting to design a cathode for Ca batteries that closely resembles the intercalation chemistries of better-known metals like Li, Na, or Mg is not feasible due to the intricate crystal chemical analogies [42].

The second category of cathode materials are compounds that perform conversion reactions[54]. Here the reactions are not topotatic as covalent bonds are broken to form new ones between the structure and the guest during the insertion and extraction of the ion. Typically, this kind of reaction takes place during ion insertion when the electrode materials lack open channels for ion diffusion or when the number of inserted ions surpasses the maximum number of available sites. Most conversion materials are transition metal oxides, sulphides or chloride.

The energy density and the chemistry kinetic of cathodes operating with the mechanisms explained above are limited due to the volume and mass of the host structure and the poor transport of multivalent ions in solids. The factors that determine diffusion are based on crystal chemistry, where the pathways must be wide enough for ions to pass through and exhibit a favourable topology to reduce the electrostatic interactions between the diffusing cation and the lattice constituents. It is important to note that the diffusivity can significantly vary with the host composition due to coulombic repulsion between the diffusing ions and the TM cations in different oxidation states [42]. When the concentration of the working ion reaches a certain level, the increased interaction between multivalent ions is more prone to causing the arrangement of ion vacancies. This arrangement, known as ion vacancy ordering, will introduce an extra obstacle to the movement of ions due to its creation of an additional energy barrier.

Two strategies have been devised to overcome the issue of weak diffusion of divalent ions within cathodic materials. The first is to use anion with larger, more polarizable atoms such as O, S or Se in the host structure. This reduces the electrostatic interaction between the multivalent-ion and host lattice. The second strategy is to find structures in which the coordination changes along the multivalent-ion migration path are optimised. For this the preferred coordination of the ion (6 for Mg, 8 for Ca) must be avoided throughout the structure, there must be no preferred site. So, the migration barrier will be as low as possible, allowing the ions to move quickly.

4. Organic Battery materials

4.1. Advantages and Drawbacks

The idea of using organic materials to make batteries dates back to 1969[56]. It was quickly sidelined in favour of the better performing inorganic materials but has recently regained interest notably due to the lack of essential elements in the construction of LIBs. Positive electrode made of abundant elements like carbon, hydrogen, nitrogen and sulfure present several advantages (Figure 10). The crystal structure of organic battery materials (OBMs) are less sensitive to the structural changes. That means that a technology that work well with one ion is easily transposable to another one.

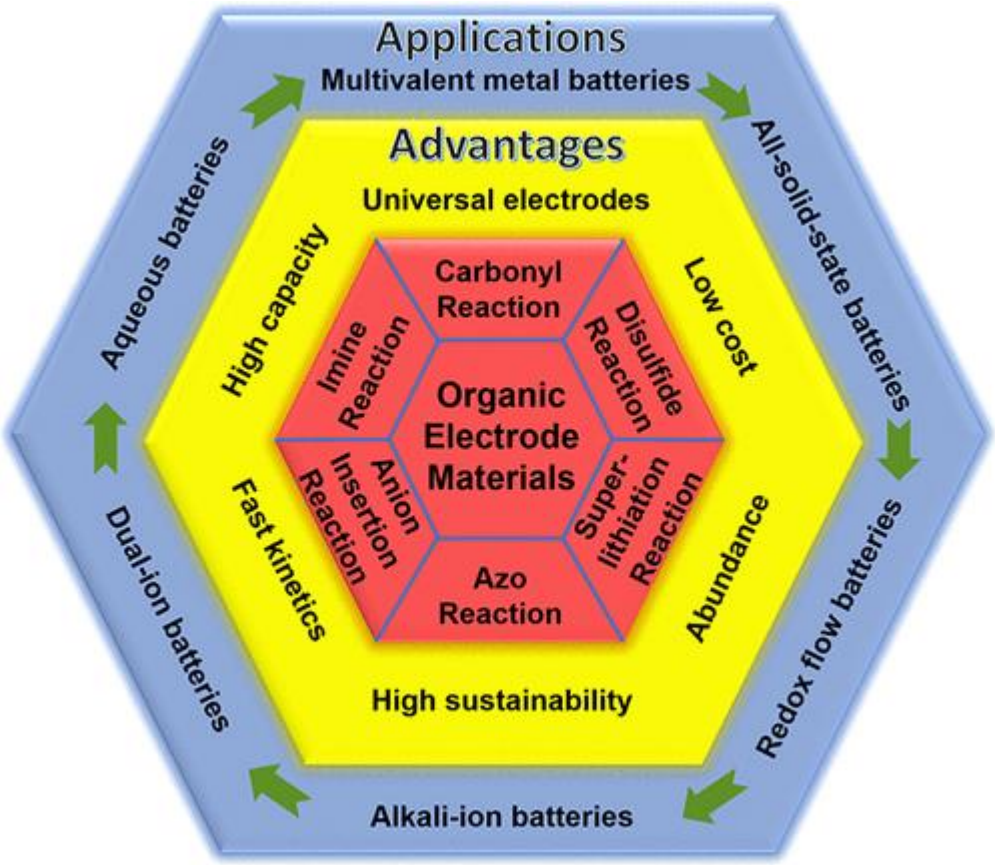

Figure 10: Application, advantages and reaction in OBMs extracted from [57].

Organic molecules possess the advantageous properties of tunability and adaptability. This enables the design of various classes of molecules with diverse redox potentials and specific capacities, making them suitable for applications as both anodic and cathodic materials in batteries. Moreover, these organic molecules can be utilized in either solid-state or dissolved form, providing flexibility in battery design and fabrication.

The production of organic molecules, even if derived from petroleum, is still less polluting compared to the extraction of cobalt or other rare metals. Furthermore, some of these organic molecules can be manufactured through green chemistry processes [3]. Their environmentally friendly composition is another notable advantage. When subjected to thermal treatment, organic molecules can be thermally destroyed without emitting odours or generating dust or toxic particles, making battery disposal processes safer and cleaner [58].

On the other hand, they have some drawbacks compared to inorganic materials. The active materials are more likely to dissolve in the electrolyte causing a loss of capacity, they are poor electrical conductors thus increasing the required amount of conductive additive. This amount of redox inactive material lowers the total specific capacity of the mixture. They also have a lower density and therefore a lower volumetric capacity and their thermal stability range is narrower.

4.2. The Different Families of Electrodes Materials

It exists many reaction mechanisms in the OBM chemistry. Depending on the type of reaction, they can be classified into three main groups (Figure 11).

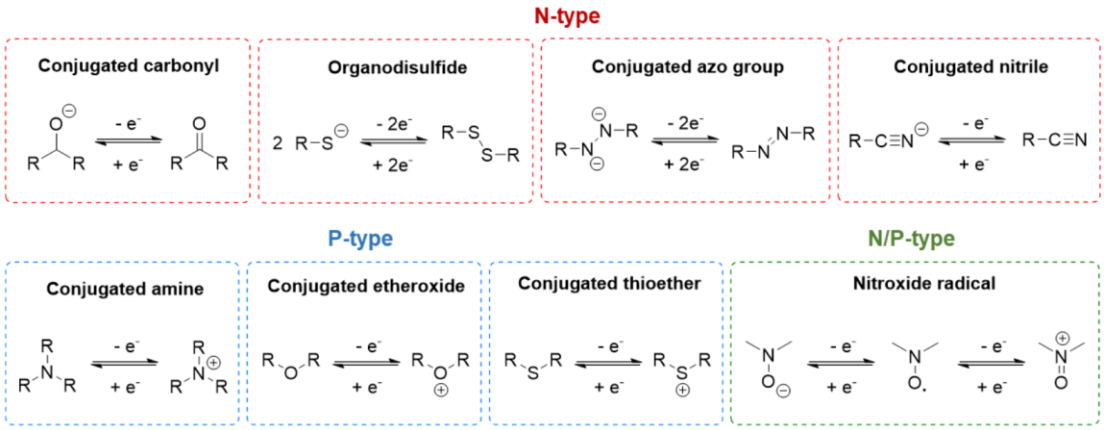

Figure 11: Families of organic cathode materials, readapted from [59].

N-type materials [60] belong to a group of compounds where the process of reduction starts from a neutrally charged oxidized state and progresses to a negatively charged state. To balance the negative charge, positively charged cations from the electrolyte are necessary. These materials have a wide range of redox potentials, making them suitable for use as both cathode and anode material.

The second group is the P-type compounds. In contrast with N-type materials, their reduced form is electrically neutral. When they undergo oxidation, a positive charge is produced which is balanced by taking up anions (such as PF_6^-, $TFSI^-$, BF_4^-, ClO_4^-, etc.) from the electrolyte. These chemistries have a high redox potential, but their specific capacity is generally lower than that of N-type materials due to the higher molecular weight of the redox active materials and the stored anions.

The final group is a blend of N-type and P-type chemistry, involving a neutral, positive, and negative state in the electrochemical process. This group has received less attention and relies solely on the chemistry of nitroxide radicals.

OBMs offer significant potential for use in a wide range of EESS due to their remarkable electrochemical performance but also for other distinctive features, such as flexibility, processability, and structural diversity. We can cite rechargeable batteries that use other ions that lithium that we will discuss more in details in section 6.2 but also, thin film, all-solid batteries and aqueous and redox batteries.

5. Conjugate Sulfonamide

A new family of OBM, known as conjugated sulfonamides (CSA), was discovered in 2021 by Vlad *et al*. [61]. These materials meet the requirements of positive electrode materials for Li-ion batteries i.e. be prepared in a reduced (anionic) form containing Li. The synthesis of these materials was inspired by lithium bis(fluorosulfonyl)imide (LiFSI) and lithium bis(trifluoromethanesulfonyl)imide (LiTFSI) salts, which are already widely used in battery chemistry. The idea was to use the electron delocalization through the sulfonyl groups to reduce the nucleophilicity of the nitrogen centre, making the otherwise highly reactive N-Li bond resistant to hydrolysis and oxidation.

The main challenge in using these materials was to achieve a reversible redox reaction. To address this challenge, a Wurster-type redox agent was used to bind to the sulfonamide function, which stabilizes it when it undergoes oxidation. Therefore, the simplest CSA material, Li_2-p-PDSA (dilithium 1,4-phenylenebis((methylsulfonyl)amide)) (Figure 12) was synthesized using this approach. This material can operate at high voltage (>3 V vs Li^+/Li_0) while avoiding decomposition. Unlike other OBMs, this molecule demonstrated exceptional stability, remaining intact even after exposure to ambient air for six months. Additionally, it maintained its integrity when dissolved in water and subsequently recrystallized.

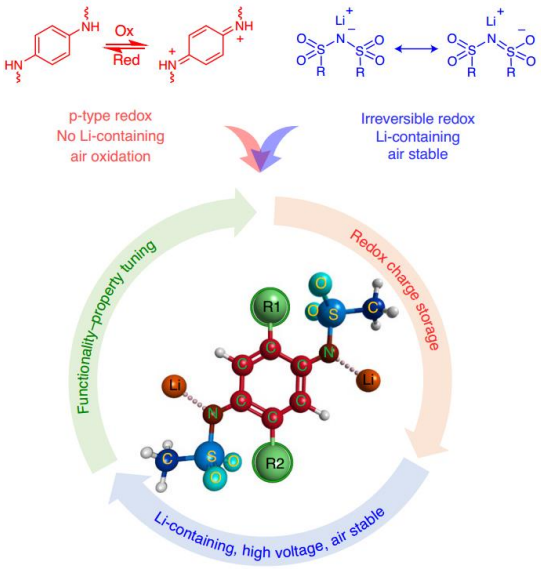

Figure 12: The molecular design of CSA Li-ion positive electrode materials draws inspiration from two organic chemistry concepts—the reversible redox of phenylene-di(poly)-amines merged with the sulfonamide functionality, extracted from [61].

Driven by the excellent results shown by this molecule, other similar products have been synthesized and the protocol has been optimized to be done in two steps: sulfonation of aromatic (conjugated) amines followed by proton-Li exchange. With this, the influence of stereoisomerism, multiredox centres and substituent electron effects on the electrochemical properties and charge-storage performances could be analysed.

It has been shown by cyclic voltammetry that the mechanism of the redox reaction of these compounds in liquid phase is a two-electron sequential oxidation to the quinoneimine (Figure 13). When in its reduced anionic form, the negative charge of the conjugated sulfonamide system is delocalized throughout the entire system, including the aromatic core. This results in a decreased interaction between the cation and anion compared to ionic compounds with more localized anion charges. The delocalization of the negative charge also enhances the electrochemical stability and increases the redox potential, as the nucleophilicity of the nitrogen atom is decreased. When there are several sulfonamide groups around the aromatic ring their placement plays an important role in the reversibility and voltage of the redox process.

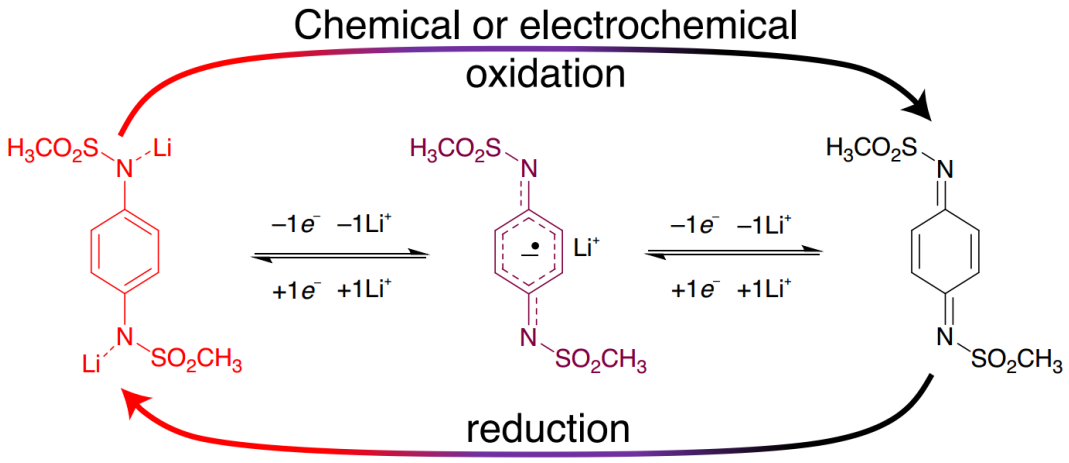

Figure 13: Schematic of the reversible two-electron redox process in dilithium 1,4-phenylenebis((methylsulfonyl)amide), extracted from [61].

In the solid state the two oxidation reactions take place in one step at a potential above 3 V vs Li^+/Li which makes it a high-performance cathode material compared to other organic compounds for LIB. In addition, it seems that the redox potentials exhibit higher values when they are measured in the solid phase compared to when they are measured in liquid phase.

6. Use CSA for Post-Li Technologies

6.1. Use with Other Monovalent Ions

In 2023, Vlad et al. extended their discovery on lithium benzene-1,2,4,5-tetra-methylsulfonamide (Li_4-PTtSA) to other alkali metals [62]. The Na_4/K_4-PTtSA derivatives can be prepared using a similar procedure as that for the lithium derivative. This involves grafting the methanesulfonyl groups, followed by sodiation/potassiation using stoichiometric amounts of sodium/potassium methoxide in anhydrous methanol under an inert atmosphere. The structure analysis, as well as the physicochemical and electrochemical properties, yield valuable insights for individuals interested in utilizing sulfonamide for NIB or KIB applications.

All the compounds showed an electrical conductivity greater than 10^{-8}C/cm at RT and it is mainly due to a hopping type of mechanism (Figure 14). Under the effect of the electric field a cascade of redox reactions occurs between the electrons of the Lowest Unoccupied Molecular Orbital (LUMO) of one molecule and the Highest Occupied Molecular Orbital (HOMO) of the neighbouring molecule. The electrons "jump" from one molecule to an the other until they reach the positive electrode.

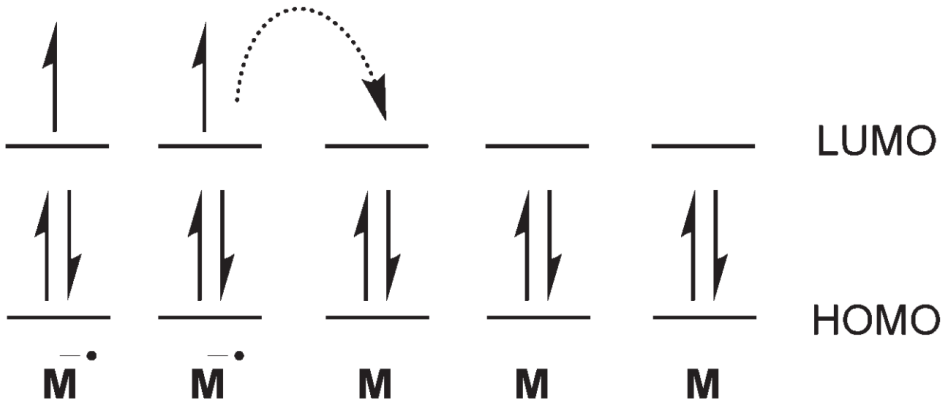

Figure 14: Hopping model where the transport of electrons is achieved by chemical oxidation/reduction, extracted from [63].

The ability of metals to exert polarizing power, which is related to the charge of the spectator cation and its radius, enables the manipulation of electron density and consequently the measurement of the redox potential of the organic molecule to which it is bonded. These changes are directly observable by ^{1}H-NMR and infrared analysis.

In 2022, Vlad et al. used recent findings on sulfonamides to create new coordination polymers with the composition of A_2-TM-PTtSA (A = Li^+, Na^+, K^+; TM = Fe^{2+}, Co^{2+}, Mn^{2+}) [64]. Its synthesis is very simple and is done in one step. The presence of transition metals in the chain enables a considerable enhancement of the materials' electronic conductivity, achieving values in the range of 10^{-6} and 10^{-7} $S.cm^{-1}$ at RT which is comparable to the value of inorganic materials. Compounds that showed higher crystallinity and long-range order obviously presented a better conductivity. It can be assumed that charge conduction occurs primarily through a through-bond mechanism, wherein electron self-exchange takes place between the redox active TM centers and the organic linkers or by electron hoping. Among all the compounds synthetised Li_2-Co-PTtSA shows the highest conductivity. This is probably due to a stronger interaction and electron self-exchange between the d-electrons of the metal and the π-electrons of the ligand that have good orbital overlapping and a small energy level difference.

This molecule has several advantages over other coordination polymers (CPs). Firstly, the presence of cobalt in the polymer chain induces a bigger polarisation of the PTtSA linkers, enhancing their redox potential by as much as 1 V when compared to the parents A_4-PTtSA. These materials exhibit redox potential values that are among the highest ever reported for organic cathode materials.

The A_2-Co-PTtSA CPs showed a reversible capacity of approximately 100 $mAh.g^{-1}$ with a 96.5% capacity retention over 1.000 cycles at a scanning rate of 5C. The data indicate two plateaus in the charge-discharge cycles at 2.85 V and 3.40 V vs Li^+/Li. In an attempt to understand this phenomenon, a comparison of the structural and elemental analyses of the oxidised and reduced materials was established. The researchers were then able to prove that the CP reaction mechanism shown on Figure 15. In this case the oxidation state of the metal does not change, the two-electron reversible redox is only centered on the organic ligand.

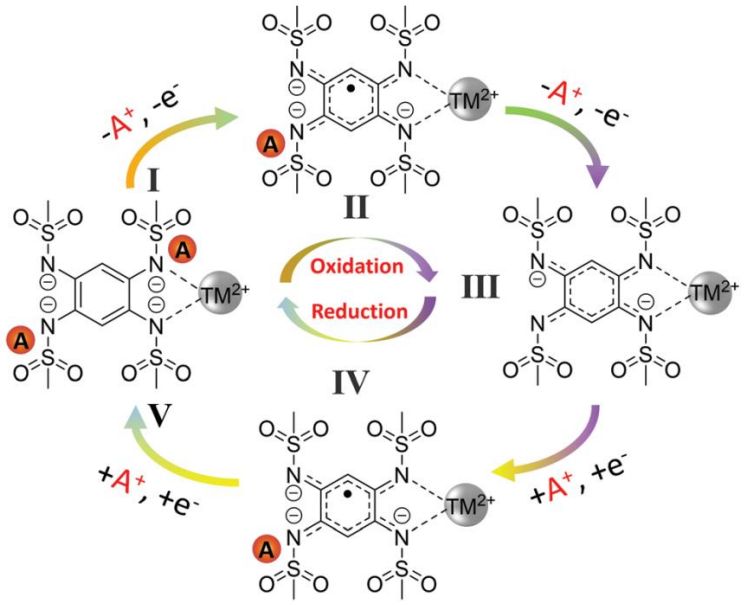

Figure 15: Redox reaction mechanism of A_2-TM-PTtSA. Extracted from [64].

The excellent rate capability and cycling stability measurements were also reported (Figure 16) even at low carbon content (5 wt%) and high mass loading (50 mg.cm^{-2}) which makes it a material of choice for CP as cathode materials.

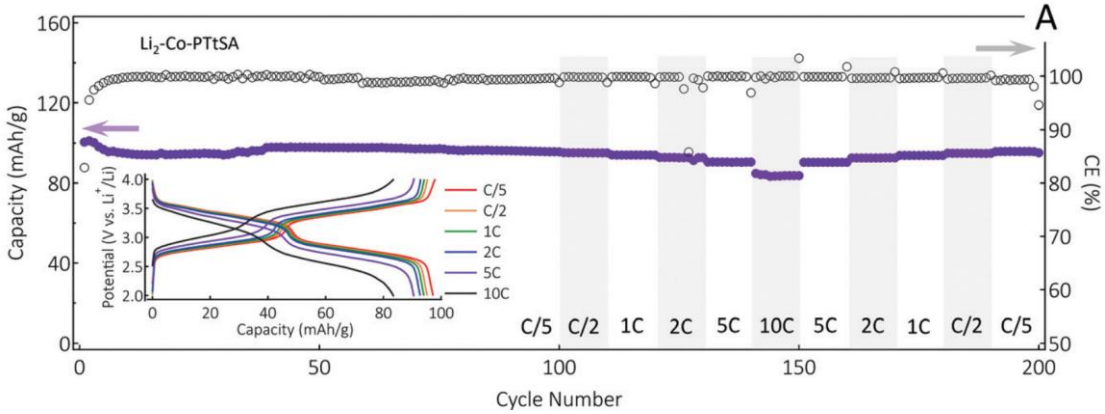

Figure 16: Cycling stability of Li2-Co-PTtSA measured at different cycling rates ranging from C/5 to 10C, with the corresponding charge-discharge profiles shown in the inset and Redox reaction pathway of A2-TM-PTtSA. Extracted from [64].

Furthermore, the electrochemical properties of the Na and K-ion analogues are comparable, indicating again that the OBMs are universally applicable to any relevant alkali-cation battery chemistry [64].

6.2. For Bivalent Ions

After demonstrating the feasibility and performance of CP derived from sulfonamide materials with alkali metals, Vlad et al. extended their new knowledge to other TMs but also to alkali-earth metals [65], [66].

The electrical conductivity of Mg-Co-PTtSA and Ca-Co-PTtSA is between 10^{-8} and 10^{-9} S/cm, which is 10 to 100 times lower than for their alkali metal counterparts. The calcium based CP exhibits a remarkable storage capacity of approximately 97 $mAh.g^{-1}$ while maintaining excellent capacity retention and operating at an average potential higher than 3 V compared to Ca^{2+}/Ca. On the other hand, when utilizing a 0.1 M $Mg(ClO_4)_2$ in EC:PC electrolyte for Mg^{2+}, a more rapid loss of capacity is observed. This is attributed, at this stage, to the heightened solubility of the oxidized form of Mg-Co-PTtSA.

The utilization of Ketjenblack carbon (KB) brought about a significant improvement in the capacity retention of the Mg-Co-PTtSA material. This enhancement can be attributed to several factors. Firstly, the adsorbent nature of carbon KB ensures a strong interaction with the active components of the material, allowing for better retention of their capacity over time. Moreover, by utilizing this derivative of graphite instead of super P (SP), the oxidized component remains on the surface rather than being dissolved or lost during the electrochemical processes. By mitigating solubility concerns, KB carbon ensures a higher capacity retention for the Mg-Co-PTtSA material, enhancing its overall performance and longevity.

To eliminate the use of cobalt, the researchers explored alternative sustainable divalent cations such as iron (Fe^{2+}), manganese (Mn^{2+}), nickel (Ni^{2+}), zinc (Zn^{2+}), and magnesium (Mg^{2+}) [66]. They measured the conductivity of all the new compounds and observed that the conductivity of Co^{2+}, Fe^{2+}, Mn^{2+} and Ni^{2+} based CP was higher than of Zn^{2+} and Mg^{2+} ones. This discrepancy is probably due to difference in electronic structure of the redox innocent $3s^0$ for Mg^{2+} and $3d^{10}$ for Zn^{2+} and redox-active $3d^x$ of other metals.

By using redox innocent metals like Zn^{2+} and Mg^{2+} in the chain and by following the changes in electrochemical responses (charge-discharge profiles) they tried to establish a better understanding of the redox reaction mechanism of CP. Indeed, the possibility of oxidation of the binder metal to Co^{3+} was not yet been completely dismissed. Unfortunately,

the structural information of these compounds is difficult to analyse by Powder X-Ray Diffraction Analysis (PXRD) due to the low phase crystalinity.

Galvanic measurements showed that the retention of CP capacity was better when Zn was used to bind the monomers rather than cobalt. Ca-Zn-PTtSA is 90% after 50 cycles while Ca-Co-PTtSA is only 83%. Its colombic efficiency is also better. It is 83% for the first cycle and 99% for the 49th cycle for Ca-Zn-PTtSA against 81% and 102% for Ca-Co-PTtSA. This columbic efficiency higher than 100% could be due to a redox shuttle mechanism by means of a chemical compound capable of moving without reacting chemically. Another approach to solving the structure of the Ca-Zn-PTtSA and the Ca-Co-PTtSA was to synthesise the complexes shown in Figure 17 and compare their structure with the corresponding CP by Extended X-Ray Absorption Fine Structure (EXAFS) and X-ray Absorption Near Edge Structure (XANES). The crystal structure of the two complexes was found to be very similar. In both cases the metal centre is coordinated to the 4 nitrogens of the sulfonamide entities in a tetrahedral configuration induced by the steric hindrance around Co^{2+} and Zn^{2+}caused by the bulk-size of the four $-SO_2CH_3$ groups.

Figure 17: Small complexes for structural information of Ca-M-PTtSA. Extracted from [66].

Further structural analysis of the oxidised and reduced form of Ca-Co-PTtSA confirmed the extraction and insertion of Ca^{2+} probably coordinated to the polymer oxygens during cycling.

VI. Outlook and Scope

As described in the previous section, CSA materials represent promising materials for addressing the challenges associated to renewable energy storage. This is due to their excellent performances in terms of energy storage capabilities, sustainability, and abundance of constituent elements.

In terms of energy storage, multivalent ions exhibit high charge densities, which enable them to achieve theoretical capacities greater than those attainable with monovalent ions. This property is crucial for developing batteries capable of storing large amounts of energy in small and lightweight systems.

In order to get a better understanding of the performance and behaviour of CSA materials containing divalent ions, further research and characterization are essential. To do so, we will compare the structures, compositions and electrochemical behaviours of all A-Zn-PTtSA derivatives (A = Mg, Ca, Sr, Ba). The compounds will be synthesized at RT or in solvothermal bomb following a similar route shown on Figure 19. H_4-PtTSA will be synthesized from benzene-1,2,4,5 tetraamine. Then, we will deprotonate the amine with lithium methoxide and zinc chloride will be added to bind the ligand together. Finally, lithium will be replaced by divalent metals by simple cation exchange reaction.

To ensure the drying efficiency of the desired powder materials and the success of the last step of the synthesis, these will be characterized by elemental analysis and Fourier Transform Infrared Spectroscopy (FTIR). The shifts of the absorption bands of the sulfonamide functionalities will also enable to observe the interactions with the cations in the structure. The crystallinity of the compounds will be determined by PXRD.

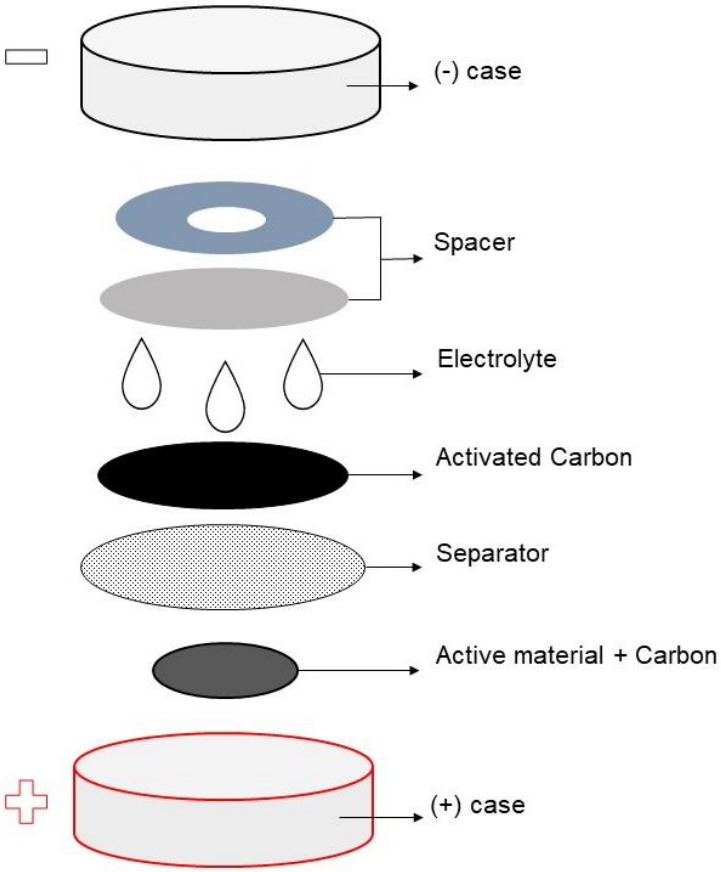

Figure 18: Coin cell use in this paper.

For the electrochemical performance experiments, the assembly of the electrochemical cells were realized as schematized in Figure 18. On the positive electrode, the active material mixed with carbon super P or KB was added a separator. Acarbon sheet were used to act as the negative electrode then wetted the whole with the electrolyte solution containing the ions. Then we closed the system and we placed it on a cycler that will charge and discharge the battery in a loop. During the charging process we monitored potential to extract the capacity.

VII. Results

1. Synthesis

The alkaline earth CP were synthesized in a one pot reaction based on the procedure established by A. Vlad et al. for Ca-Zn-PTtSA[64]. The different synthesis steps are shown schematically in Figure 19. The journey starts with the synthesis of the organic linker, H_4PTtSA, which is obtained through a nucleophilic substitution from the 1,2,4,5-benzene tetraamine. The purity of the linker is determined based on the Nuclear Magnetic Resonance(^{1}H-NMR) spectra (see supporting information section 1-2 for more details) and is above 99%. The ligand is then deprotonated using lithium methoxide (MeOLi), followed by two cation exchanges: the first one with $ZnCl_2$ in order to create the coordination polymer, and the second with ACl_2 (A = Mg, Ca, Sr, Ba) to replace Li^+ by A^{2+}. Finally, the cation exchange reaction was performed at RT and at 100°C in a solvothermal bomb to study the impact of the synthesis temperature on the structural and electrochemical performances of the CP.

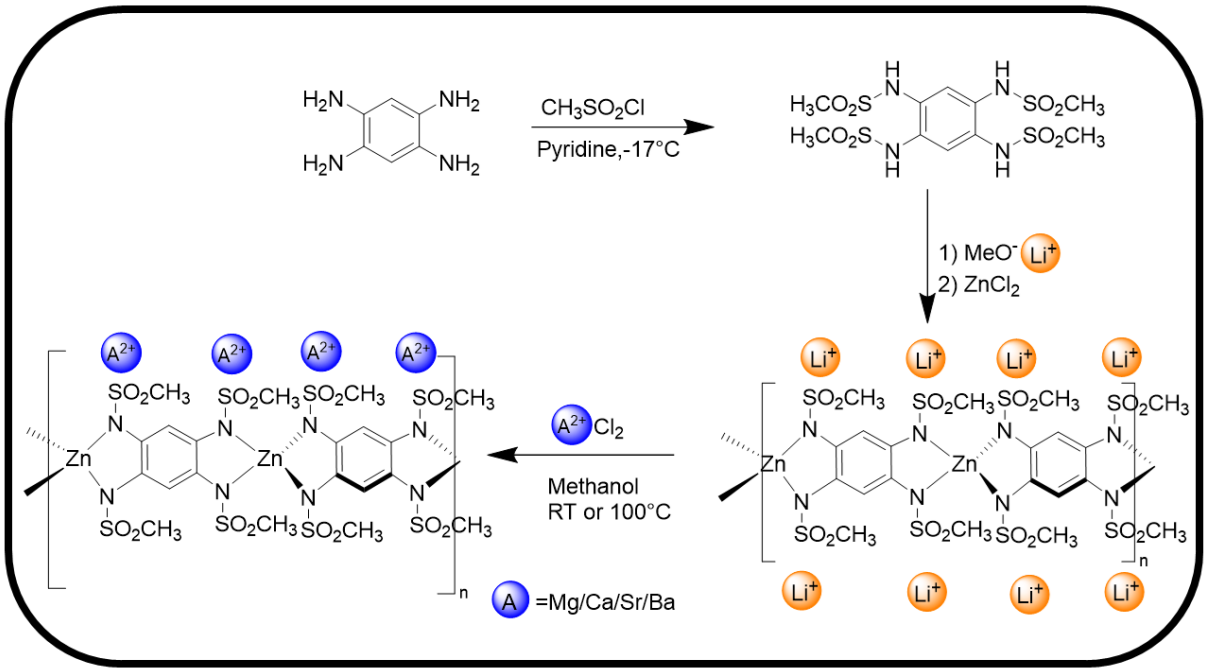

Figure 19: Synthesis of A-Zn-PtTSA derivatives.

The synthesis of A-Zn-PTtSA compounds were performed based on the reagents and quantities reported in Table 1 (details in supporting information). Under argon atmosphere (Glove box), 100 mg of H_4-PTtSA (0.22 mmol, 1.0 equiv.) and 33.71 mg of lithium methoxide (0.8878 mmol, 4.0 equiv.) were dissolved in 10 ml of methanol in a 20 ml vial. After stirring for 1 hour, 30.25 mg of zinc chloride (0.22 mmol, 1.0 equiv.) compound was dissolved in 1 ml of methanol and then added dropwise to the reaction medium and the solution were felt under stirring for 24 hours. The corresponding alkaline-earth chloride (0.44 mmol, 1.0 equiv.) were dissolved in 1 ml of methanol and added dropwise to reaction medium. In solvothermal bomb reactions, all the reagents were added at the same time.

An instant pink precipitate was forming. After an addition day of stirring, the reaction medium was centrifuged and washed 3 times with methanol and 3 additional times with diethyl ether. The powder is finally dried in a vacuum oven at 180°C for 14 hours. The completeness of the drying was verified by FTIR. If the band at 3500 cm^{-1} was still present, the sample was re-dried at a higher temperature.

Table 1: Equivalent of reagent for the polymerisation and the cation exchange reaction. The reaction has been done in methanol.

Chemical		Equivalent
N, N', N'', N'''-(benzene-1,2,4,5-tetrayl)tetramethanesulfonamide (H_4-PtTSA)		1
Lithium methoxide		4
Alkaline-earth Chloride	**$MgCl_2$**	1
	$CaCl_2$	1
	$SrCl_2$	1
	$BaCl_2$	1
Zinc chloride ($ZnCl_2$)		1

2. Characterization

2.1. Fourier transform Infrared Spectroscopy

Since the polymers are insoluble in most common solvents, ^{1}H-NMR could not be performed to study the structure of the ending products. Therefore, the success of the reaction and the drying of the product were monitored by FTIR. The drying temperature was optimized for all polymers based on the disappearance of the methanol bands, 3400 cm^{-1} the FTIR spectra (Figure 20).

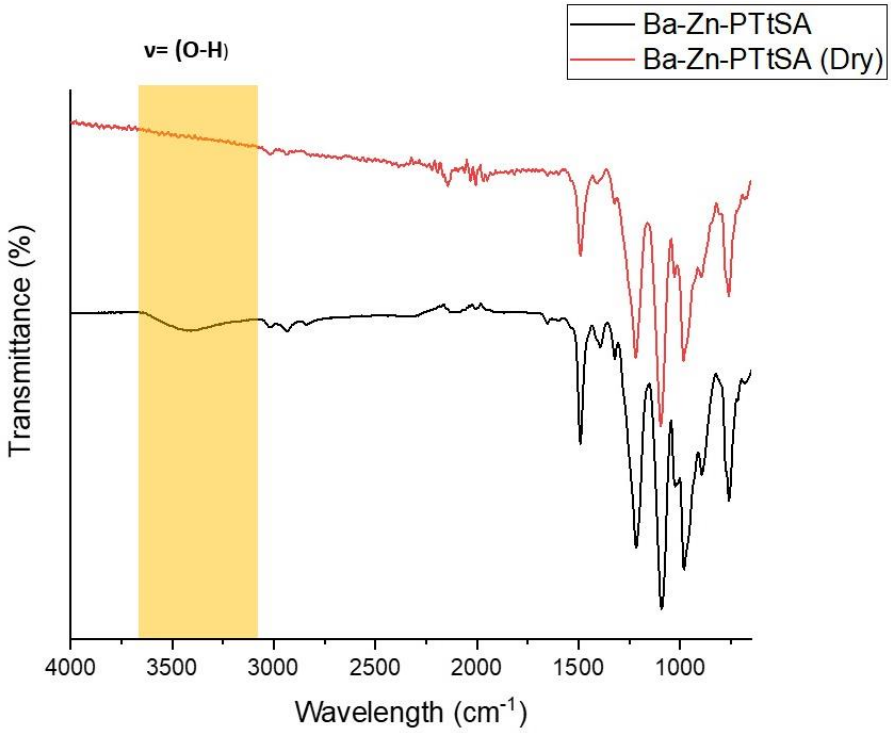

Figure 20: Ba-Zn-PTtSA before and after drying.

Several conclusions can be drawn when comparing the spectra of the CPs to the spectrum of the organic linker, and to each other (Figure 21). A significant finding is the absence of the N-H stretching band, typically appearing at approximately 3100 cm^{-1} in H_4-PTtSA, across all CPs, which suggests the complete deprotonation of the ligand within these compounds. In addition, all the CP spectra look similar to each other and to what was reported in the literature, confirming the formation of the desired compounds.

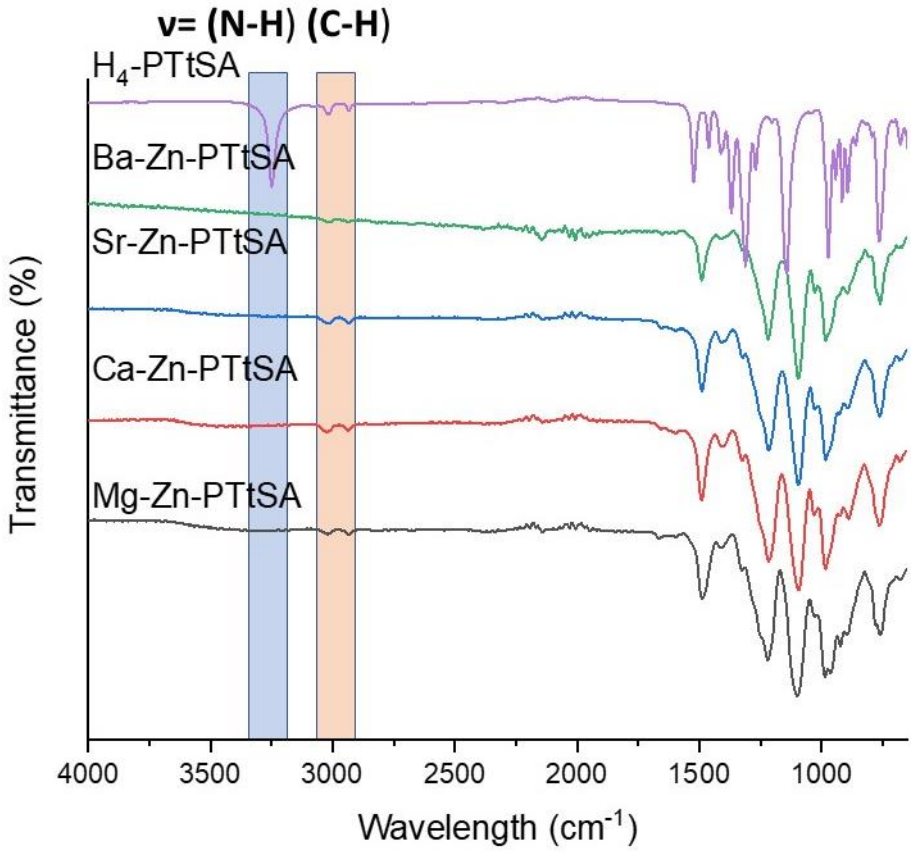

Figure 21: FTIR spectra of sample synthetised at RT.

A second important observation can be made when zooming in on the low wavelength range of the spectrum (Figure 22), between 1750 and 650 cm^{-1}. The vibrational bands of (S=O), initially observed at 1312 and 1114 cm^{-1} for H_4-PTtSA, have been shifted to 1218 and 1095 cm^{-1} in the case of all the CPs. This can be explained by the coordination of the metal cations to the sulfonamide entities, which again confirm the formation of CPs. However, while the shift is evident when comparing to the organic linker, no significant difference in S=O band position can be observed between the CPs.

In a previous research, Vlad *et al.* observed a significant shift in S=O but only when changing the coordination cation (TM = Fe^{2+}, Co^{2+}, Zn^{2+} and Ni^{+2}), which was attributed to the strong binding of TM to the sulfonamide entities and the difference in their polarizing power [64]. In Na_2-Co-PTtSA and K_2-Co-PTtSA, alkaline cations were found to remain localized at the periphery of the chain, comparable to the arrangement observed in complex similar to Ca-Zn-PTtSA compound.

Since the position of the S=O depends on the coordination environment, this suggests two things: (i) Zn^{2+} is coordinated in the same ways in all the coordination polymers and (ii) the alkaline earth cations are weekly bond to the sulfonamide group, and so to the polymer. We can therefore assume that most of these are not involved in the polymer chain but are rather located in its surroundings.

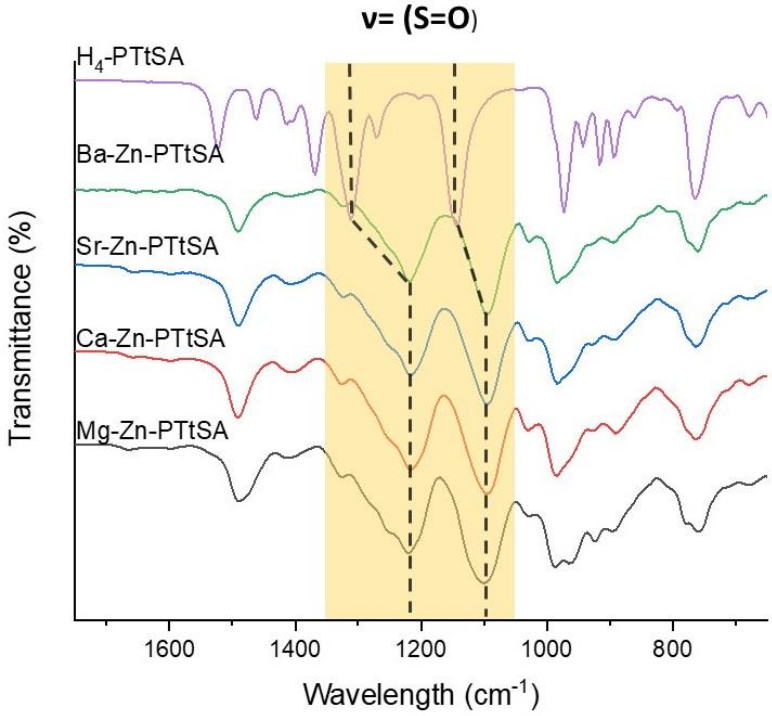

Figure 22: Zoom for IR at room temperature.

2.2. Elemental Analysis

CHNS elemental analyses were performed on the samples synthesized at RT to verify their purity and to ensure that there is not solvent left in the CPs (Table 2). It can be observed that the percentage of carbon and hydrogen in the samples is systematically a little higher than the theoretical percentage, while this trend is reversed for nitrogen and sulphur. This could be explained by the presence of a small amount of residual methanol in the coordination polymers, in sufficiently small quantities that could not be detected by FTIR. The difference could also come from the impurities present in the organic linker since this one is not 100% pure, such as (tri/bi) substituted sulfonamide (and not tetrasubstituted). The presence of residual lithium in the compound can also interfere with the analysis results. Additional analysis, such as the composition in oxygen, are required in order to confirm these conclusions.

Table 2: Elemental analysis (C, H, N, and S mass percentages) of the compounds synthetised at room temperature.

		C(%)	N(%)	H(%)	S(%)
Mg-Zn-PTtSA	Theory	22.40	10.45	2.63	23.92
	Results	21.42	9.10	2.47	20.86
Ca-Zn-PTtSA	Theory	21.76	10.15	2.56	23.23
	Results	20.93	9.21	2.71	21.42
Sr-Zn-PTtSA	Theory	20.04	9.35	2.35	21.39
	Results	19.46	8.49	2.52	19.8
Ba-Zn-PTtSA	Theory	18.50	8.63	2.17	19.75
	Results	18.48	7.92	2.41	18.44

In order to study the efficacity of the cation exchanges reaction and the impact of the synthesis temperature, inductively coupled plasma- optical emission spectrometry (ICP-OES) analyses were performed on all the samples to evaluate the amounts of Li^{+}, Zn^{2+} and A^{2+} in the coordination polymers. Using the mass percentages measured, we were able to calculate the proportion of each metal in the theoretical formula for the compound (Table 3).

Table 3: Mass percentage of each metal determined by ICP-OES and conversion to stoichiometric ratio. The boxes corresponding to samples whose measurement has probably been missed are framed in red.

A=		**$[Li_xA_yZn_z](PTtSA)$**								
		$\%m_{th(Li)}$	**$\%m_{exp(Li)}$**	**x**	**$\%m_{th(A)}$**	**$\%m_{exp(A)}$**	**y**	**$\%m_{th(Zn)}$**	**$\%m_{exp(Zn)}$**	**z**
Mg	RT	0	0.20	0.19	4.53	3.29	0.90	12.19	9.82	1.00
	100°C		0.66	1.05		0.08	0.04		8.56	1.44
Ca	RT	0	0.21	0.19	7.26	6.28	0.96	11.85	10.04	0.94
	100°C		0.13	0.12		6.44	1.01		9.63	0.93
Sr	RT	0	0.18	0.17	14.62	12.75	0.93	10.91	10.14	0.99
	100°C		0.06	0.06		11.94	0.96		9.41	1.01
Ba	RT	0	0.02	0.02	21.15	18.13	0.98	10.07	8.85	1.01
	100°C		0.04	0.04		17.31	0.89		10.07	1.09

Where $\%m_{th}$ is the theoretical mass percentage of the simplified repeating unit (Figure 23) used to model the coordination polymers and $\%m_{exp}$ is the experimental mass percentage.

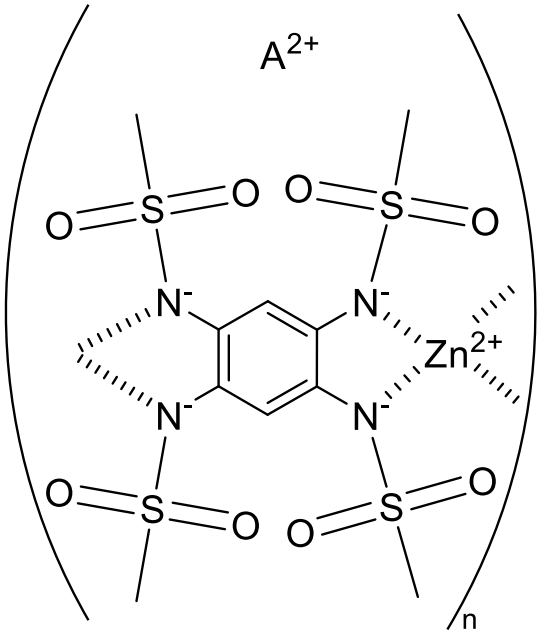

Figure 23: Theoretical repeating unit of A_2-Zn-PTtSA.

In order to determine the x, y, and z values, our calculations (detailed in the supporting information section 3) were based on the assumption that all the metals detected exist as cation and that their positive charges balance out the four negative charges from the deprotonated ligand. This means that we disregard the presence of other anions, such as MeO^-, Cl^-, and OH^-, in the sample. The key aspect of this calculation is to accurately quantify the relative proportions of different metals present.

The disparity between the theoretical and practical mass percentages in ICP-OES can be attributed to the presence of impurities in the samples, as elucidated by the CHNSO analyses but especially by the presence of residual lithium. Indeed, it can be observed that lithium is systematically present in a non-negligible amount for all the samples, indicating that the cation exchange is not 100% efficient.

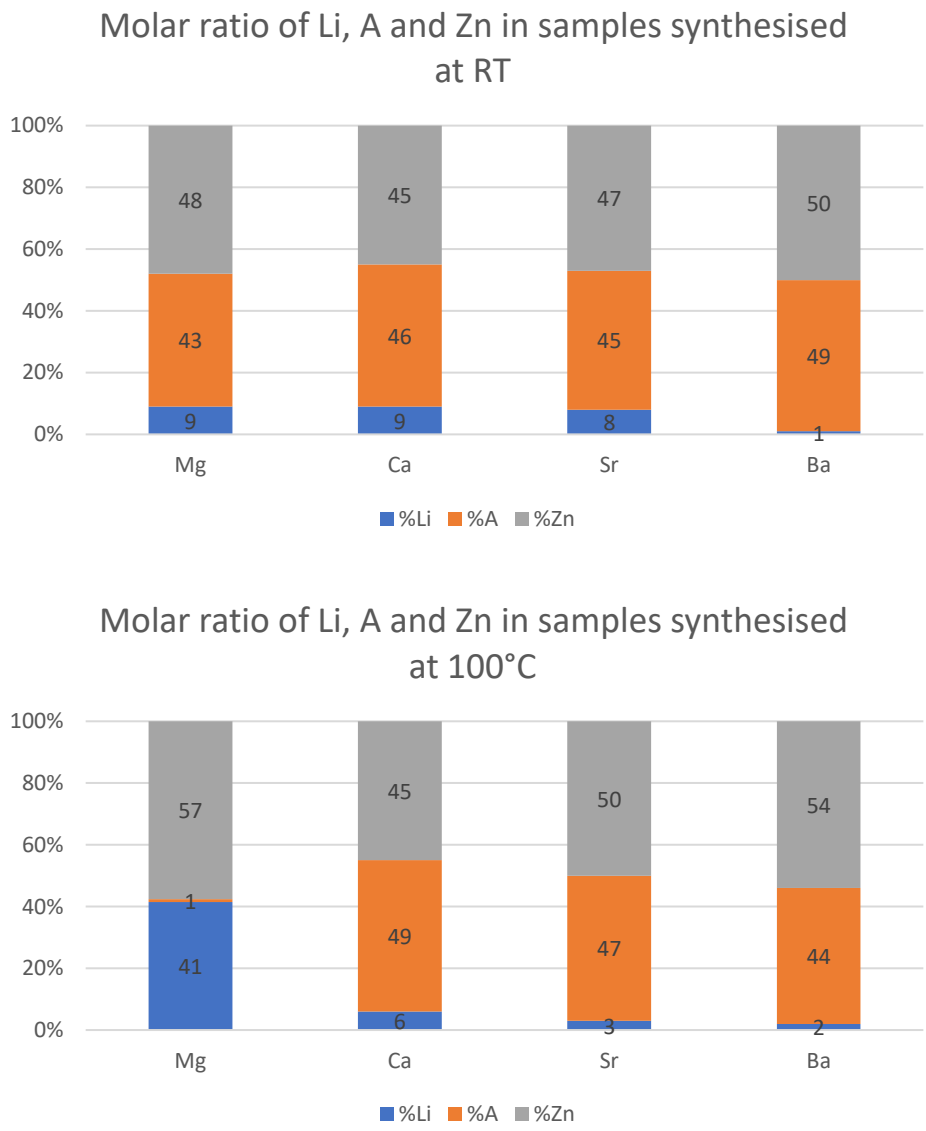

Figure 24: Graph of the atomic ratios of the elements Li,A,Zn in the A-Zn-PTtSA (A=Mg,Ca,Sr,Ba) samples.

The Li/(TM+M) ratio shows a decreasing trend when transitioning from Mg^{2+} to Ba^{2+} (Figure 24). This could suggest a potential improvement in cation exchange efficiency, although the observed trend is quite subtle and lacks strong statistical significance. These graphs also clearly demonstrate that there was some confusion observed during the testing of the sample of Mg-Zn-PtTSA synthesized at a temperature of 100°C.

2.3. Powder X-Ray Diffraction Analysis

One of the purposes of this systematic study of alkaline earth derivates was the hope that one of them will be enough crystallin to enable a structural resolution. However, as shown in Figure 21, the absence of intense and distinct diffraction peaks in the patterns of all height samples indicates a poorly crystalline nature. However, the broad and similar amorphous patterns observed suggested that calcium and magnesium compounds share an iso-amorphic structure. In the same way, there were similarities observed in the poorly crystalline patterns of Sr-Zn-PTtSA and Ba-Zn-PTtSA. In addition, increasing the synthesis temperature doesn't improve much the crystallinity of the CPs. Due to this poor crystallinity, extracting structural information from the PXRD data remains impossible.

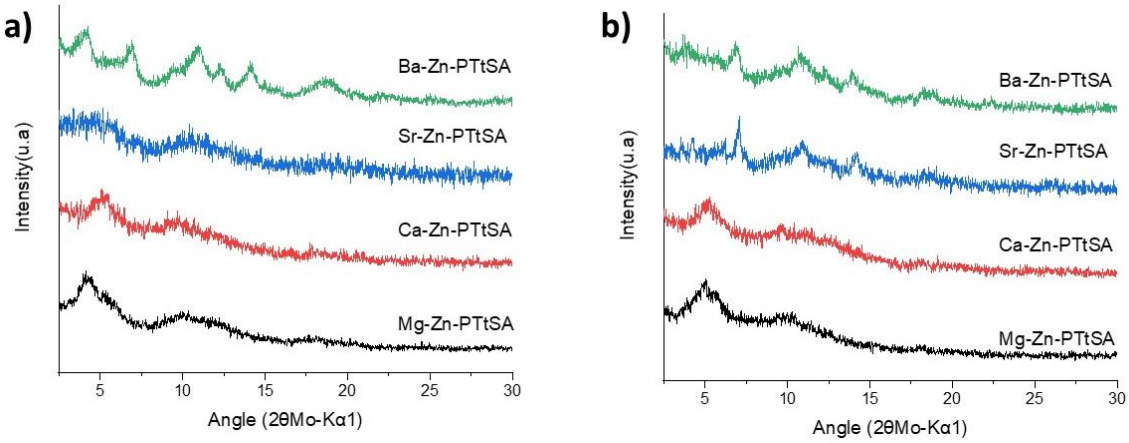

Figure 25: PXRD for samples synthetised at a) Room Temperature and b) at 100°Cl.

2.4. Galvanic Measurement

Finally, as Ca-Zn-PTtSA was reported to have impressive performances as cathode material for calcium batteries, an electrochemical study was performed on all the coordination polymers to see if these are compatible with other systems.

Initially, we compared the performance of 0.5M $Ca(TFSI)_2$ and $Mg(TFSI)_2$ solutions in DME. However, we couldn't compare these results with other metals like $Sr(TFSI)_2$ and $Ba(TFSI)_2$ because those salts were not accessible. As a solution, we decided to evaluate batteries using perchlorate salts instead. Unfortunately $Sr(ClO_4)_2$ and $Ba(ClO_4)_2$ are not soluble in DME. We therefore chose to test this solution in Diethyl Carbonate (DEC) and inEthyl Methyl Carbonate (EMC).

Since all the tested materials demonstrated the ability to function in batteries, we aimed to find a new electrolyte composition that could be universally applicable to all alkaline earth metals for better comparison. However, this task proved challenging due to difficulties in achieving salt solubility with the available solvents. After a comprehensive investigation, we made an interesting discovery that all alkaline earth perchlorates were soluble in acetonitrile. Additionally, we noticed that cells utilizing this solvent exhibited remarkable performance. All the cycles in this solvent are shown in the supporting information section 6.

Since the OBMs are characterized by a low electrical conductivity, i.e. 10^{-10} $S.cm^{-1}$ in the case of the previous reported Ca-Zn-PTtSA, these are usually mixed with a significant amount of conductive carbon. In this work, an electrode composition of 50% of dirired CP:40% SP-carbon:10% of Polytetrafluoroethylene (PTFE) was used.

We also tested our cells with a formulation containing 60% of KB instead of super P, but improvement in performance was not always observed. Indeed, due to its ability to adsorb ions from the surrounding medium, KB enhances the density capacity of the medium by approximately ten mAh/g. This occurrence leads to the formation of a slope at the commencement and conclusion of each galvanic measurement.

Consequently, distinguishing whether the observed enhancement in measured performance is a result of this adsorption or if KB has genuinely prevented the solubilization of the CP can be challenging. Nonetheless, there are instances where this distinction is clear, such as with barium-based samples synthetised at RT, for instance (Figure 26).

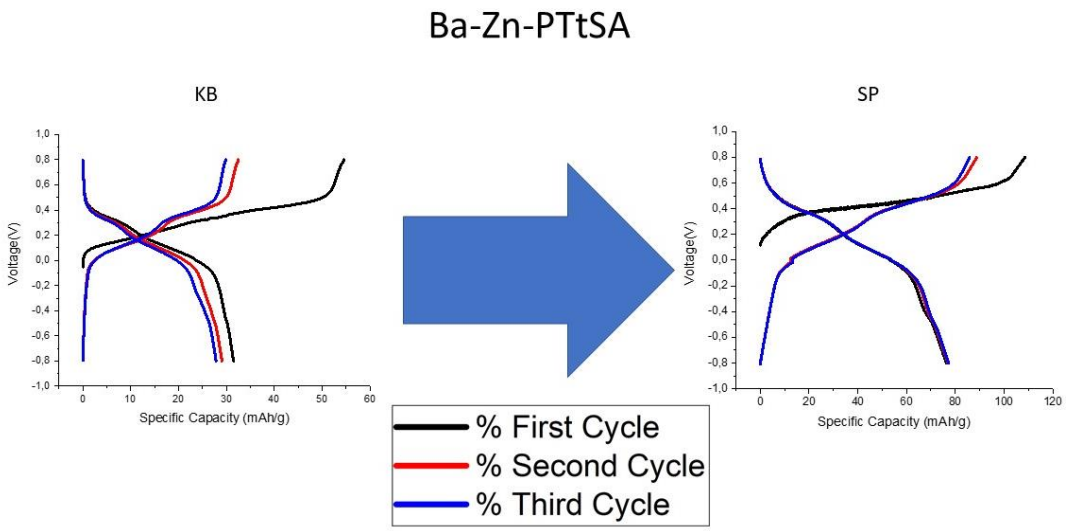

Figure 26: Clear improvement in the density capacity of the Ba-Zn-PTtSA sample when carbon SP is replaced by carbon KP.

The increase in specific capacity associated with changing the type of carbon is primarily noticeable in samples synthesized at RT. It is probable that the structure of these samples is more susceptible to solubilization during the cycling process. This susceptibility may be attributed to shorter polymer chains or a weaker degree of interaction between them.

Since the metal anodes cannot be used as counter electrode in the systems studied here, these were replaced by carbon clothes, already reported as being an efficient alternative for post-Li technologies[67].

It can be often seen that the specific capacity measured in the first cycle is always much higher than that measured in the second and third cycle (Figure 27). A good explanation for this phenomenon is that during the first cycle the lithium and other impurities remaining in the materials after the synthesis is also extracted. There could also be structural changes in the material, which would reduce its capacity.

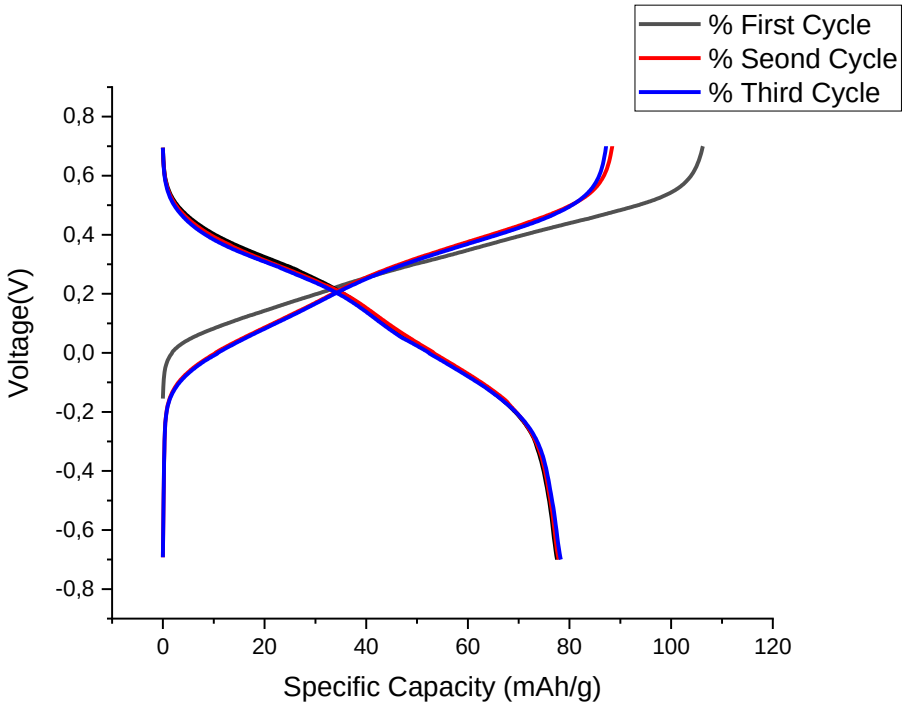

Figure 27: Cycling of Ca-Zn-PTtSA.

Now we can compare the performances of the sample done with both synthesis at different temperatures for each metal (Figure 28). At RT, the samples synthesized with calcium exhibit significantly higher specific capacity compared to their counterparts. Surprisingly, this calcium-based samples even surpass the performance of samples synthesized at high temperatures, which generally show superior specific capacity. Setting aside this anomaly, we can explain this trend by considering that high-temperature synthesis promotes the formation of polymers with varying sizes. Depending on the size of the polymer, the compound tends to facilitate the exchange of surrounding cations more readily.

When larger cations such as strontium and barium are involved, the redox mechanism appears to occur in two distinct steps. This can be observed through the presence of two distinct waves when measuring the specific capacity. However, this phenomenon is less apparent with smaller cations and is not observed when testing monovalent ion batteries.

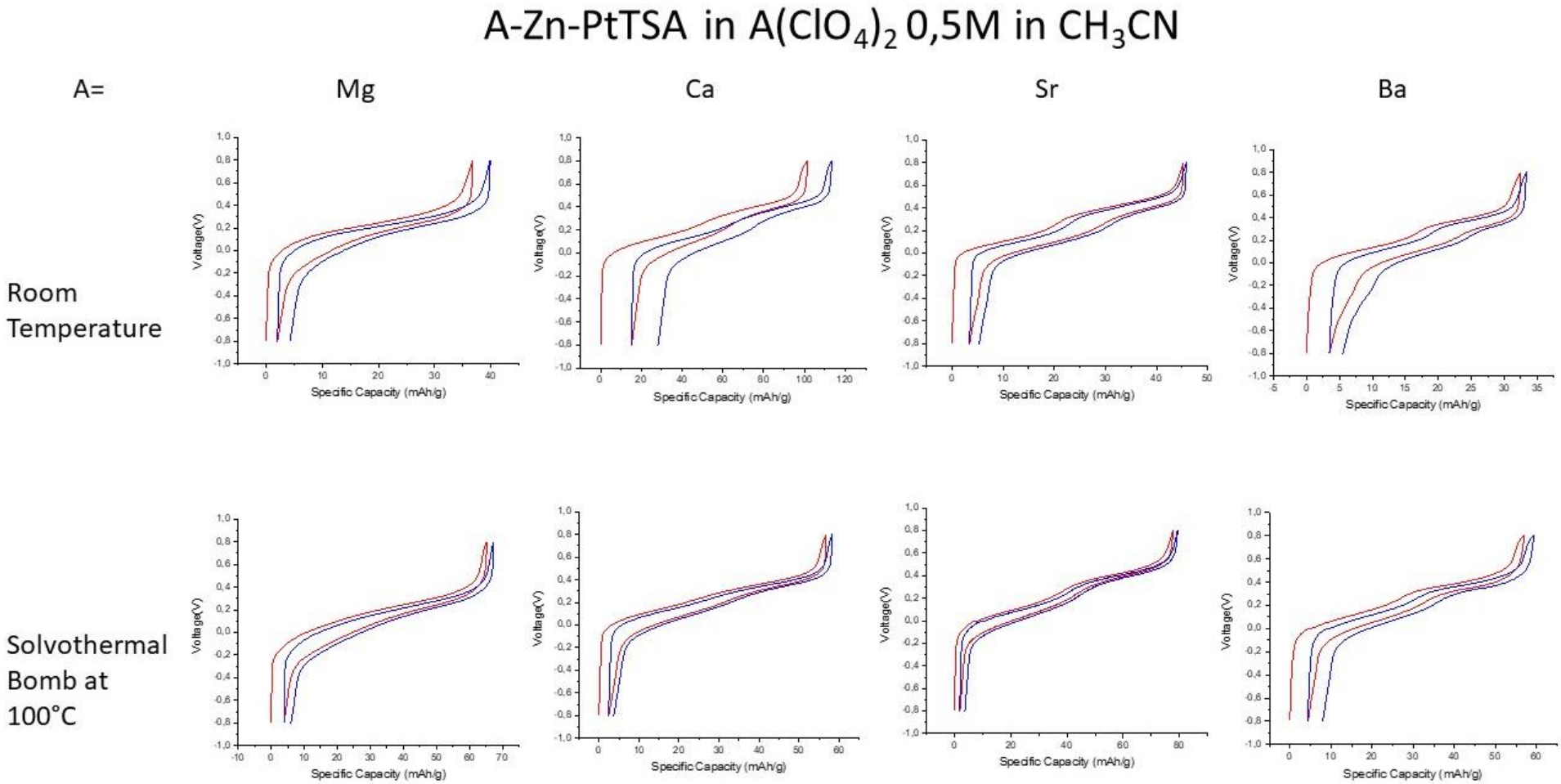

Figure 28: Comparison of the butterfly diagrams of all the A-Zn-PtTSA in 0.5M $A(ClO_4)_2$ in CH_3CN synthetised with both methods at Room Temperature or at 100°C in a solvothermal bomb.

With the exception of the magnesium-based sample synthesized at RT, all the other samples exhibited a decrease in specific capacity with each cycle (Figure 29). This decrease is likely caused by the dissolution of the oxidized phase of the polymer in the electrolyte. In contrast, the RT-synthesized magnesium-based sample showed a reversal of this trend, indicating that structural changes occur within the sample during cycling. The columbic efficiency of all the samples is between 90 and 100%, which is a decent performance for OBMs. Unfortunately, due to time constraints, we were unable to perform 10 cycles on the calcium and strontium materials as planned.

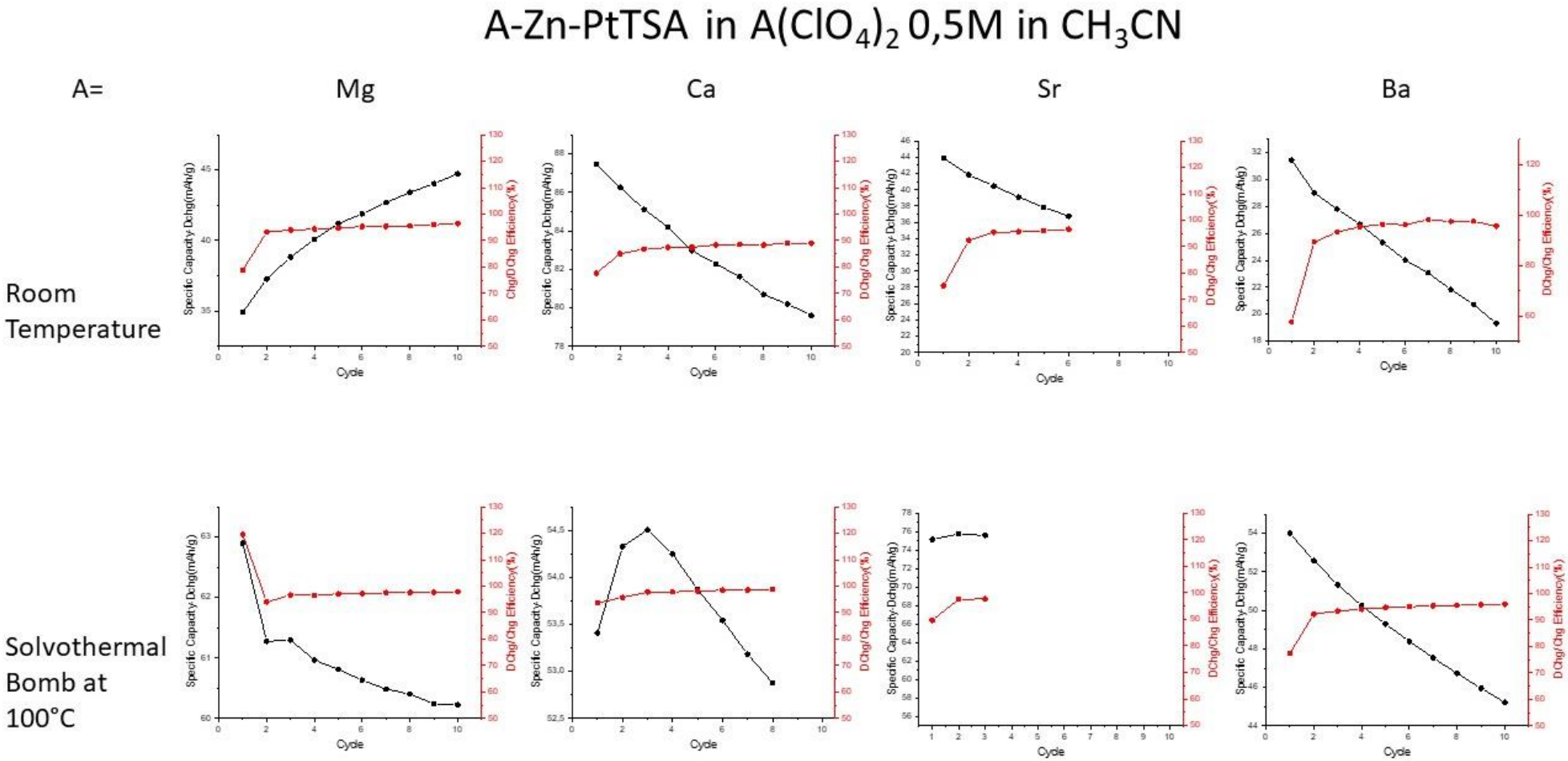

Figure 29: Comparison of charge-discharge efficiency for all the A-Zn-PtTSA in 0,5M $A(ClO_4)_2$ in CH_3CN synthetised with both methods at Room Temperature or at 100°C in a solvothermal bomb.

VIII. Conclusion and Perspectives

To summarize, the successful synthesis of the ligand is indicated by the similarity of the infrared spectra. However, determining the proportion of ligands coordinated with Zinc compared to other metals remains a challenge. When the alkaline-earth cation was altered in the A-Zn-PTtSA formula, no shift in the absorption bands was observed. This suggests that these cations, which possess distinct polarizing abilities, remain in the CP chain environment without being incorporated into it.

The elemental analysis and ICP-OES indicate incomplete cation exchange reactions with no clear temperature-dependent trend observed. Heavier atoms seem to have a tendency to replace lithium more easily.

Furthermore, the XRD analysis indicates that the crystal structures of magnesium and calcium samples, as well as strontium and barium samples, remain similar regardless of the synthesis temperature. However, samples synthesized at higher temperatures exhibit an enhanced specific capacity, implying differences between room temperature and high temperature synthesis. It is plausible that the temperature is correlated with the size of the polymer chains. This correlation could explain why substituting carbon Super P with carbon KB in cells increases the capacity of cathodic materials A-Zn-PTtSA materials synthesized at room temperature.

Lastly, the use of acetonitrile as an electrolyte proves advantageous, as it dissolves all $A(ClO_4)_2$ salts, facilitating effective material comparison. Additionally, this electrolyte enables a higher degree of reversible cation extraction.

In summary, while the infrared spectra, elemental analysis, XRD analysis, and electrolyte selection provide valuable insights into the synthesis, crystal structures, and electrochemical properties of the materials, further investigations are necessary to elucidate the precise metal bonding, temperature effects, and optimize the cathodic materials for enhanced performance.

Future research should focus on addressing these aspects and expanding the knowledge in the field. One potential avenue is the use of solid-state nuclear magnetic

resonance to gain insights into the metal-ligand interactions and coordination chemistry, providing a deeper understanding of the specific metal binding and proportions in ligand synthesis. We could also make complexes similar to CPs and analyse them by EXAF and XANES to find out more about the position of the cations within the compounds.

Additionally, in-depth analysis of the materials at the nanoscale using techniques such as transmission electron microscopy (TEM) or scanning probe microscopy (SPM) can offer valuable information on the morphology, particle size, and distribution within the synthesized materials, further enhancing the understanding of their structure-property relationships.

To achieve complete cation exchange, future research should explore alternative reaction conditions, such as different temperatures, solvent, or reaction times.

Furthermore, utilizing advanced techniques such as ex-situ FTIR for cation solvation, C-rate analysis for cation extraction, and Galvanostatic Intermittent Titration Technique (GITT) for cation diffusion can provide a more comprehensive understanding of the electrochemical behaviour of the synthesized materials. These techniques can shed light on solvation dynamics, kinetics, and transport mechanisms, ultimately contributing to the design of materials with enhanced electrochemical performance and stability.

By incorporating these research directions, it is possible to deepen our understanding of cation extraction, solvation, and diffusion within the synthesized materials. This knowledge will drive the development of sustainable and efficient energy storage technologies, supporting the transition to cleaner and more renewable energy resources.

IX. Supporting Information

1. Synthesis

a) N, N', N'', N'''-(benzene-1,2,4,5-tetrayl)tetramethane-sulfonamide (H_4-PTtSA)

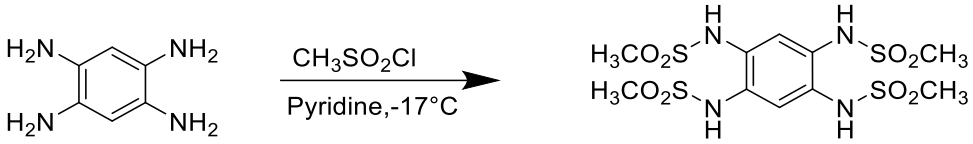

Chemical	Mw (g/mol)	Mass (g)	d(g/ml)	Moles(mol)	Equivalent
1,2,4,5-Benzenetetramine tetrahydrochloride	284.01	2.48		0.01	1
1,2,4,5-Benzenetetramine Tetrahydrochloride	113.95		1.48	0.04	4
Pyridine					50 mL

2.48 g of 1,2,4,5-Benzenetetramine tetrahydrochloride (0.01 mol, 1.0 equiv.) was added into around bottom flask (100 mL) with 50 mL of pyridine and cooled to -17°C with an ice/salt bath. Then, 3.1 ml of methanesulfonyl chloride (0.04 mol, 4.0 equiv.) was then slowly added drop wise in 30 minutes. After the addition, the ice/salt bath was removed and the solution was left to slowly warm up to RT under stirring for 24 hours. After this, 200 mL of 1M HCl was added to the solution. The precipitate was filtrated and then washed 3 times with 100 mL of 1 M HCl and 3 times with 100 mL of water, resulting in a light pink powder of N, N', N'', N'''-(benzene-1,2,4,5-tetrayl)tetramethane-sulfonamide. The powder was dried under vacuum at 70°C.

b) Coordination polymer (A_2-Zn-PTtSA)

The synthesis is explained in detail on page 31. Table 4 gives a precision on the quantities used.

Table 4: Reagents and quantities used for the synthesis of the A_2-M-PTtSA coordination polymers.

Chemical		Mw (g/mol)	Mass (mg)	V(ml)	Moles(mmol)	Equivalent
N, N', N'', N'''-(benzene-1,2,4,5-tetrayl)tetramethanesulfonamide (H_4-PtTSA)		450.51	100		0.22	1
Lithium methoxide		37.91	33.71		0.8878	4
Alkaline-earth Chloride	**$MgCl_2$**	95.21	21.13		0.22	1
	$CaCl_2$	110.98	24.63		0.22	1
	$SrCl_2$	158.53	35.18		0.22	1
	$BaCl_2$	208.23	46.22		0.22	1
Zinc chloride($ZnCl_2$)		136.3	30.25		0.22	1
Methanol				10		

2. ^{1}H-RMN

1H NMR spectra were performed by a 300 MHz Bruker Advance II.

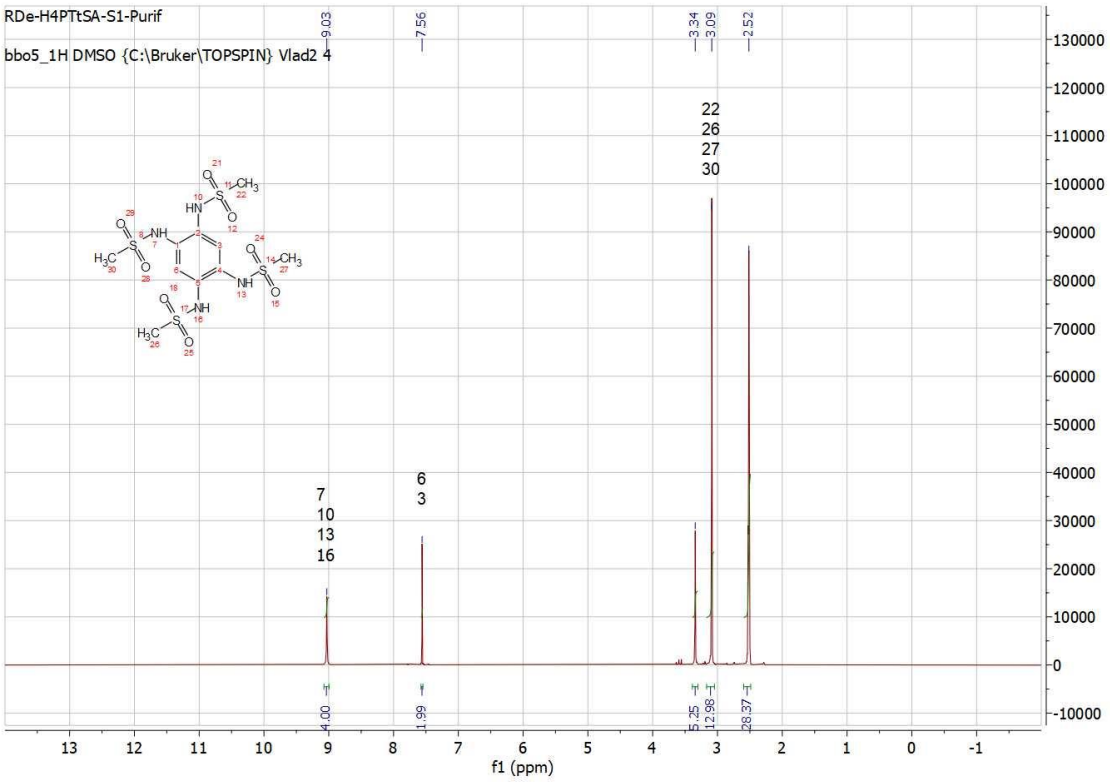

Figure 30: ^{1}H NMR in DMSO-d_6 (300 MHz, 298 K); δ 9.03 (s, 4H), 7.56 (s, 2H), 3.09 (s, 12H).

The shift at 2.52 and 3.34 ppm correspond to DMSO and H_2O respectively.

3. Elemental Analysis and ICP-OES

MEDAC LTD company conducted inductively coupled plasma mass spectrometry analyses using a Varian Vista MPX ICP-OES system. Additionally, CHNSO elemental measurements were performed using a FlashSmart Thermoscientific CHNSO analyzer.

The calculation details for Table 3 are show on Table 5.

Table 5: Calculation details for Table 3. M_{Li}, M_A and M_{Zn} are the molar mass of their respective metal.

		C	D	E	F	G	H	I	J	K	L	M	N	O	P	Q	R	S	T	U	V	W	X
A-Zn-PTtSA		%$m_{exp(Li)}$		Li mass ratio per 1g	= mol	Molar Ratio	x	%$m_{exp(A)}$		A mass ratio per 1g	= mol	Molar Ratio	y	%$m_{exp(zn)}$		Zn mass ratio per 1g	= mol	Molar Ratio	z	%mexp (Li+A+Zn)	Total mol	Charge	Ratio to compensate for 4 charges
A=		Th	Exp	D/U	E/(M_{Li})	F/V	G*X	Th	Exp	J/U	K/(M_A)	L/V	M* X	Th	Exp	P/U	Q/(M_{Zn})	R/V	S*X	D+J+P	R+L+F	G+M* 2+S*2	4/W
Mg	RT	0	0.20	0.02	0.00	0.09	0.19	4.53	3.29	0.25	0.01	0.43	0.90	1.19	9.82	0.74	0.01	0.48	1.00	13.31	0.02	1.91	2.10
	100 °C		0.66	0.07	0.01	0.41	1.05		0.08	0.01	0.00	0.01	0.04		8.56	0.92	0.01	0.57	1.44	9.30	0.02	1.59	2.52
Ca	RT	0	0.21	0.01	0.00	0.09	0.19	7.26	6.28	0.38	0.01	0.46	0.96	11.85	10.04	0.61	0.01	0.45	0.94	16.53	0.02	1.91	2.09
	100 °C		0.13	0.01	0.00	0.06	0.12		6.44	0.40	0.01	0.49	1.01		9.63	0.59	0.01	0.45	0.93	16.20	0.02	1.94	2.06
Sr	RT	0	0.18	0.01	0.00	0.08	0.17	14.62	12.75	0.55	0.01	0.45	0.93	10.91	10.14	0.44	0.01	0.47	0.99	23.07	0.01	1.92	2.08
	100 °C		0.06	0.00	0.00	0.03	0.06		11.94	0.56	0.01	0.47	0.96		9.41	0.44	0.01	0.50	1.01	21.41	0.01	1.97	2.03
Ba	RT	0	0.02	0.00	0.00	0.01	0.02	21.15	18.13	0.67	0.00	0.49	0.98	10.07	8.85	0.33	0.01	0.50	1.01	27.00	0.01	1.99	2.01
	100 °C		0.04	0.00	0.00	0.02	0.04		17.31	0.63	0.00	0.44	0.89		10.07	0.37	0.01	0.54	1.09	27.42	0.01	1.98	2.02

4. Infrared Analysis

Agilent Technologies' Cary 630 FTIR spectroscopy system, was utilized to conduct Fourier Transform Infrared Spectroscopy. The spectral range covered was from 4000 cm^{-1} to 650 cm^{-1}, with a resolution of 4 cm^{-1} and a total of 64 scans in GloveBox

5. X-ray Diffraction Analysis

Powder X-ray diffraction (PXRD) patterns were obtained using a STOE Stadi P diffractometer with a Debye-Scherrer geometry. The instrument was equipped with a Mo anticathode, which generated Kα radiation. The operating conditions for the diffractometer were set at 50 kV and 40 mA.

6. Half-cell Assembly and Testing

Electrochemical testing experiments were conducted using a Neware BTS 4000 system, employing a coin cell configuration. The negative electrode consisted of activated carbon, while the positive electrode utilized the active material. A glass microfiber filter (Whatman GF/D, Aldrich) served as the separator. For the positive electrode composition, a manual grinding process was employed, combining 50% or 60% of the active material with a conductive carbon additive (either Super P or Ketjenblack) EC-600JD from AkzoNobel), along with 10% of PTFE. The c-rate was 1/10C.

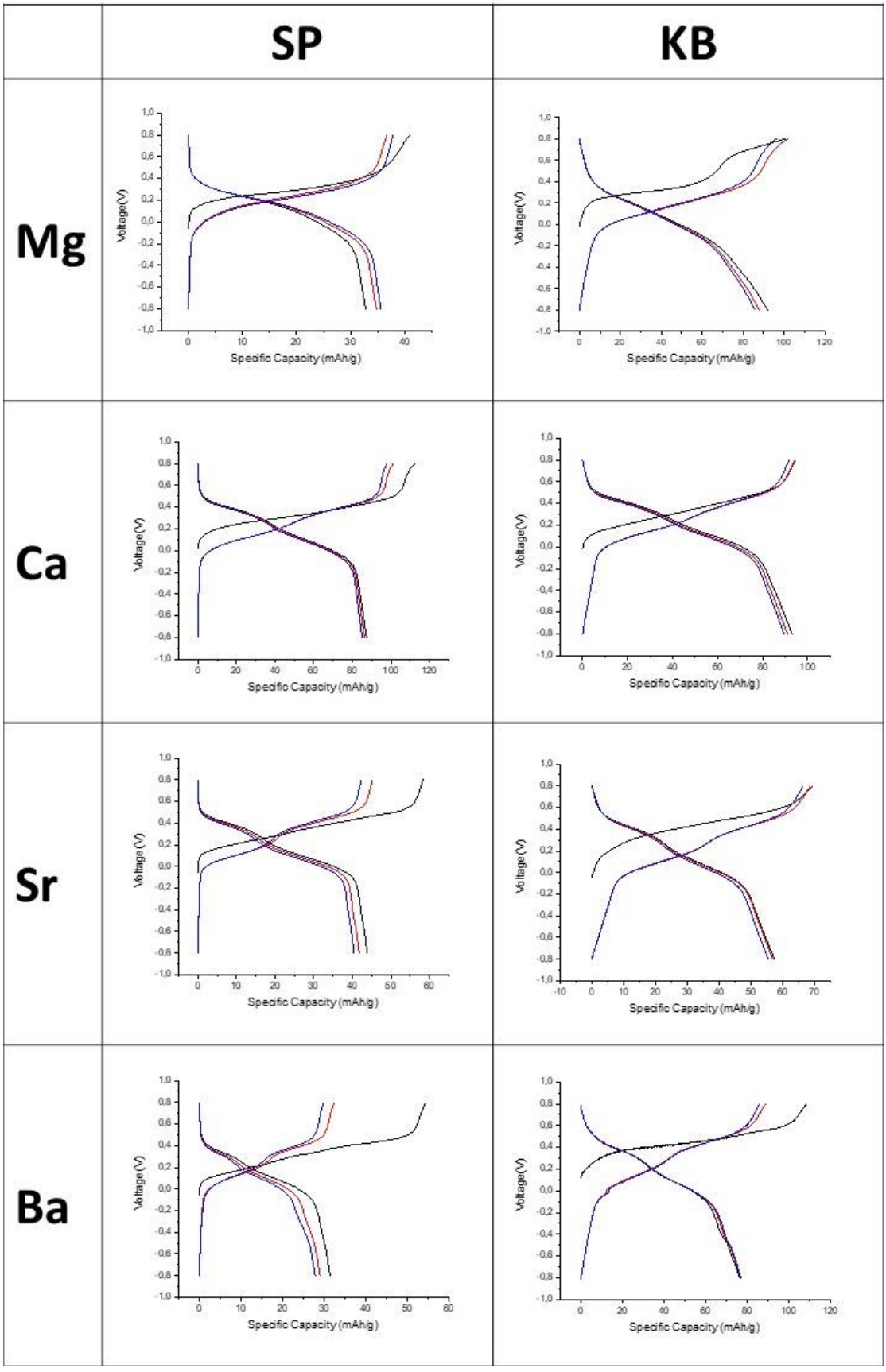

Figure 31: Comparison of specific capacity measurements of A-Zn-PtTSA samples synthesised at RT mixed with carbon SP or carbon KB .

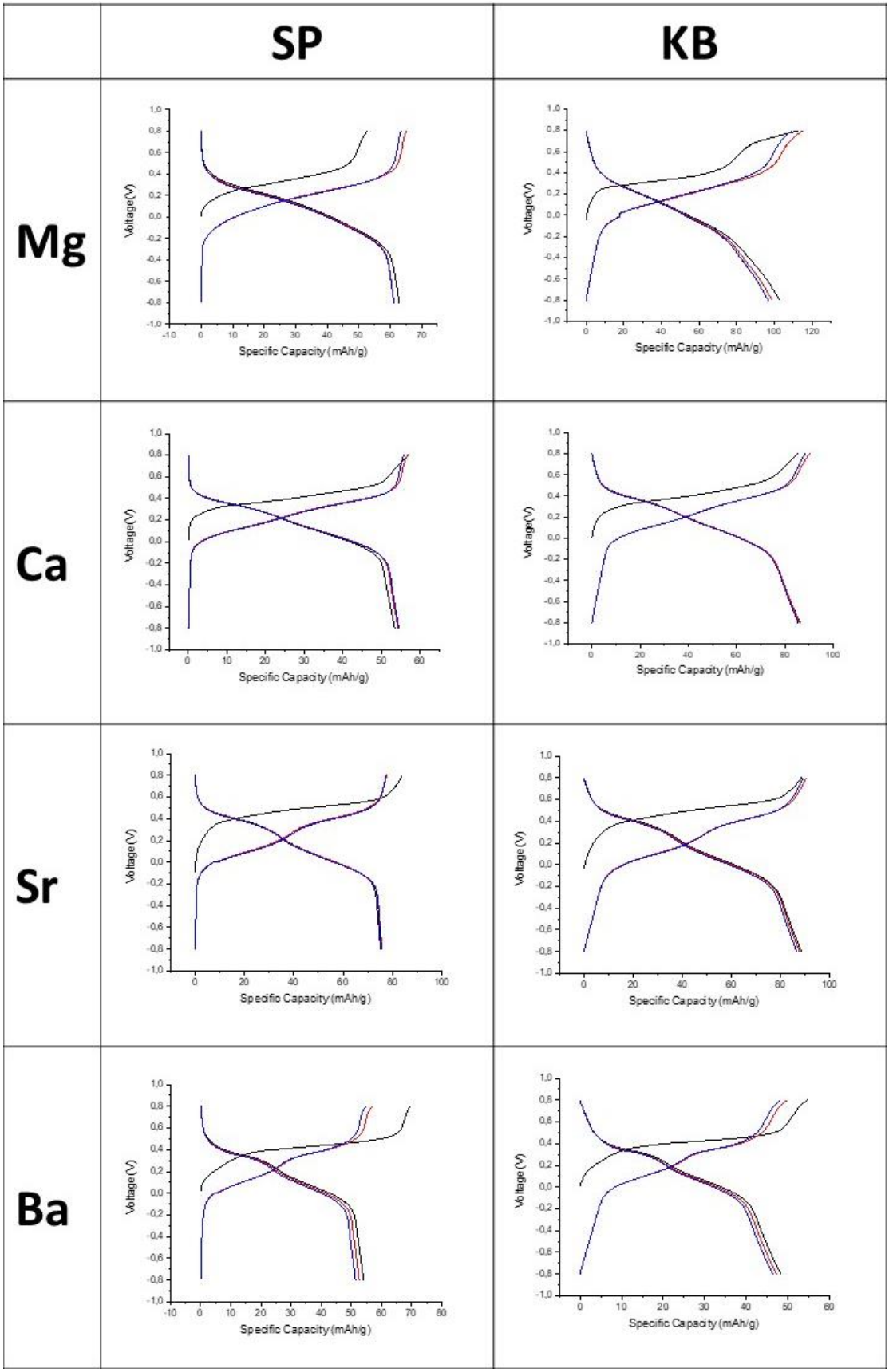

Figure 32: Comparison of specific capacity measurements of A-Zn-PtTSA samples synthesised at 100°C mixed with carbon SP or carbon KB.

X. Bibliography

1. Jean-Marc JANCOVICI. Combien suis-je un esclavagiste ? (2005).
2. Friedlingstein, P. *et al.* Global Carbon Budget 2022. *Earth Syst Sci Data* **14**, 4811–4900 (2022).
3. Poizot, P. & Dolhem, F. Clean energy new deal for a sustainable world: from non-CO2 generating energy sources to greener electrochemical storage devices. *Energy Environ Sci* **4**, 2003 (2011).
4. WINTER, N. *Renewables 2022 Global Status Report United States of America*. (2022).
5. Juvenal Alejandro, O. U. The Role of the Industrial Engineer in an Energy System Development. *Tevista de la Hacultad de Eiencias Sumicas* (2017).
6. Heiska, J., Nisula, M. & Karppinen, M. Organic electrode materials with solid-state battery technology. *J Mater Chem A Mater* **7**, 18735–18758 (2019).
7. Ferreira, H. L., Garde, R., Fulli, G., Kling, W. & Lopes, J. P. Characterisation of electrical energy storage technologies. *Energy* **53**, 288–298 (2013).
8. Larcher, D. & Tarascon, J.-M. Towards greener and more sustainable batteries for electrical energy storage. *Nat Chem* **7**, 19–29 (2015).
9. Manev, V., Ilchev, N. & Nassalevska, A. The Lithium-manganese dioxide cell I. Oxygen and water release during the thermal treatment of MnO2. *J Power Sources* **25**, 167–175 (1989).
10. Tarascon, J.-M. & Armand, M. Issues and challenges facing rechargeable lithium batteries. *Nature* **414**, 359–367 (2001).
11. Whittingham, M. S. Electrical Energy Storage and Intercalation Chemistry. *Science (1979)* **192**, 1126–1127 (1976).
12. M. Stanley. Chalcogenide battery. *U.S. Patent* **4**, 9–53 (1977).
13. Mizushima, K., Jones, P. C., Wiseman, P. J. & Goodenough, J. B. LixCoO2 (0<x<-1): A new cathode material for batteries of high energy density. *Mater Res Bull* **15**, 783–789 (1980).
14. Thackeray, M. M., David, W. I. F., Bruce, P. G. & Goodenough, J. B. Lithium insertion into manganese spinels. *Mater Res Bull* **18**, 461–472 (1983).
15. Yazami, R. & Touzain, Ph. A reversible graphite-lithium negative electrode for electrochemical generators. *J Power Sources* **9**, 365–371 (1983).
16. Megahed, S. & Scrosati, B. Lithium-ion rechargeable batteries. *J Power Sources* **51**, 79–104 (1994).
17. Manthiram, A. A reflection on lithium-ion battery cathode chemistry. *Nat Commun* **11**, 1550 (2020).
18. Li, J. *et al.* Toward Low-Cost, High-Energy Density, and High-Power Density Lithium-Ion Batteries. *JOM* **69**, 1484–1496 (2017).

19. Anderson, I. M., Haddad, P. M. & Chaudhry, I. Changes in Pharmacological treatment for Bipolar Disorder Over Time in Manchester: A Comparison with Lloyd et al. (2003). *Journal of Psychopharmacology* **18**, 441–444 (2004).

20. Tabelin, C. B. *et al.* Towards a low-carbon society: A review of lithium resource availability, challenges and innovations in mining, extraction and recycling, and future perspectives. *Miner Eng* **163**, 106743 (2021).

21. U.S. Geological Survey. *Mineral Commodity Summaries*. (2022).

22. Tarascon, J.-M. Is lithium the new gold? *Nat Chem* **2**, 510–510 (2010).

23. Baur, D. G. & Gan, D. Electric Vehicle Production and the Price of Lithium. *SSRN Electronic Journal* (2018) doi:10.2139/ssrn.3289169.

24. Martin, G., Rentsch, L., Höck, M. & Bertau, M. Lithium market research – global supply, future demand and price development. *Energy Storage Mater* **6**, 171–179 (2017).

25. Rachid Amui, J. N. *COMMODITIES AT A GLANCE: Special issue on strategic battery raw materials* . (2020).

26. Ebert, B. & Jelkmann, W. Intolerability of cobalt salt as erythropoietic agent. *Drug Test Anal* **6**, 185–189 (2014).

27. Gulley, A. L., McCullough, E. A. & Shedd, K. B. China's domestic and foreign influence in the global cobalt supply chain. *Resources Policy* **62**, 317–323 (2019).

28. OECD. *Investment Policy Reviews: China*. (2008).

29. Christophe POINSSOT. WMF CRITICALITY ASSESSMENT. in (BRGM, CRU, McKINSEY, 2022).

30. Tian, Y. *et al.* Promises and Challenges of Next-Generation "Beyond Li-ion" Batteries for Electric Vehicles and Grid Decarbonization. *Chem Rev* **121**, 1623–1669 (2021).

31. Ponrouch, A. & Palacín, M. R. Post-Li batteries: promises and challenges. *Philosophical Transactions of the Royal Society A: Mathematical, Physical and Engineering Sciences* **377**, 20180297 (2019).

32. Matsui, M. Study on electrochemically deposited Mg metal. *J Power Sources* **196**, 7048–7055 (2011).

33. Ponrouch, A. *et al.* Multivalent rechargeable batteries. *Energy Storage Mater* **20**, 253–262 (2019).

34. Liang, Y., Dong, H., Aurbach, D. & Yao, Y. Current status and future directions of multivalent metal-ion batteries. *Nat Energy* **5**, 646–656 (2020).

35. Lee, B.-S. A Review of Recent Advancements in Electrospun Anode Materials to Improve Rechargeable Lithium Battery Performance. *Polymers (Basel)* **12**, 2035 (2020).

36. Tan, Y.-H. *et al.* High Voltage Magnesium-ion Battery Enabled by Nanocluster Mg_3Bi_2 Alloy Anode in Noncorrosive Electrolyte. *ACS Nano* **12**, 5856–5865 (2018).

37. Niu, J. *et al.* Dual phase enhanced superior electrochemical performance of nanoporous bismuth-tin alloy anodes for magnesium-ion batteries. *Energy Storage Mater* **14**, 351–360 (2018).

38. Singh, N., Arthur, T. S., Ling, C., Matsui, M. & Mizuno, F. A high energy-density tin anode for rechargeable magnesium-ion batteries. *Chem. Commun.* **49**, 149–151 (2013).

39. Wang, M. *et al.* Reversible calcium alloying enables a practical room-temperature rechargeable calcium-ion battery with a high discharge voltage. *Nat Chem* **10**, 667–672 (2018).

40. Stievano, L. *et al.* Emerging calcium batteries. *J Power Sources* **482**, 228875 (2021).

41. Chen, C., Wang, J., Zhao, Q., Wang, Y. & Chen, J. Layered $Na_2Ti_3O_7$/$MgNaTi_3O_7$/$Mg_{0.5}NaTi_3O_7$ Nanoribbons as High-Performance Anode of Rechargeable Mg-Ion Batteries. *ACS Energy Lett* **1**, 1165–1172 (2016).

42. Arroyo-de Dompablo, M. E., Ponrouch, A., Johansson, P. & Palacín, M. R. Achievements, Challenges, and Prospects of Calcium Batteries. *Chem Rev* **120**, 6331–6357 (2020).

43. Gofer, Y., Turgeman, R., Cohen, H. & Aurbach, D. XPS Investigation of Surface Chemistry of Magnesium Electrodes in Contact with Organic Solutions of Organochloroaluminate Complex Salts. *Langmuir* **19**, 2344–2348 (2003).

44. Shterenberg, I., Salama, M., Gofer, Y., Levi, E. & Aurbach, D. The challenge of developing rechargeable magnesium batteries. *MRS Bull* **39**, 453–460 (2014).

45. Gaddum, L. W. & French, H. E. THE ELECTROLYSIS OF GRIGNARD SOLUTIONS [1]. *J Am Chem Soc* **49**, 1295–1299 (1927).

46. Gregory, T. D., Hoffman, R. J. & Winterton, R. C. Nonaqueous Electrochemistry of Magnesium: Applications to Energy Storage. *J Electrochem Soc* **137**, 775–780 (1990).

47. Ponrouch, A., Frontera, C., Bardé, F. & Palacín, M. R. Towards a calcium-based rechargeable battery. *Nat Mater* **15**, 169–172 (2016).

48. Shyamsunder, A., Blanc, L. E., Assoud, A. & Nazar, L. F. Reversible Calcium Plating and Stripping at Room Temperature Using a Borate Salt. *ACS Energy Lett* **4**, 2271–2276 (2019).

49. Selis, S. M., Wondowski, J. P. & Justus, R. F. A High-Rate, High-Energy Thermal Battery System. *J Electrochem Soc* **111**, 6 (1964).

50. Forero-Saboya, J. D. *et al.* Cation Solvation and Physicochemical Properties of Ca Battery Electrolytes. *The Journal of Physical Chemistry C* **123**, 29524–29532 (2019).

51. Staniewicz, R. J. A Study of the Calcium-Thionyl Chloride Electrochemical System. *J Electrochem Soc* **127**, 782–789 (1980).

52. Aurbach, D. *et al.* Prototype systems for rechargeable magnesium batteries. *Nature* **407**, 724–727 (2000).

53. D. Aurbach, R. S. Y. G. The Electrochemical Behavior of Calcium Electrodes in a Few Organic Electrolytes. *J Electrochem Soc* **138**, 3536 (1991).

54. Mao, M., Gao, T., Hou, S. & Wang, C. A critical review of cathodes for rechargeable Mg batteries. *Chem Soc Rev* **47**, 8804–8841 (2018).

55. Aurbach, D. *et al.* Progress in Rechargeable Magnesium Battery Technology. *Advanced Materials* **19**, 4260–4267 (2007).

56. Williams, D. L., Byrne, J. J. & Driscoll, J. S. A High Energy Density Lithium/Dichloroisocyanuric Acid Battery System. *J Electrochem Soc* **116**, 2 (1969).

57. Shea, J. J. & Luo, C. Organic Electrode Materials for Metal Ion Batteries. *ACS Appl Mater Interfaces* **12**, 5361–5380 (2020).

58. Nishide, H. & Suga, T. Organic Radical Battery. *Electrochem Soc Interface* **14**, 32–36 (2005).

59. Wang, J. High voltage organic positive electrode materials for alkali-ion batteries. (UCLouvain, 2020).

60. Song, Z. & Zhou, H. Towards sustainable and versatile energy storage devices: an overview of organic electrode materials. *Energy Environ Sci* **6**, 2280 (2013).

61. Wang, J. *et al.* Conjugated sulfonamides as a class of organic lithium-ion positive electrodes. *Nat Mater* **20**, 665–673 (2021).

62. Wang, J. *et al.* A High-Voltage Organic Framework for High-Performance Na- and K-Ion Batteries. *ACS Energy Lett* **7**, 668–674 (2022).

63. Volz, D. *et al.* From iridium and platinum to copper and carbon: new avenues for more sustainability in organic light-emitting diodes. *Green Chemistry* **17**, 1988–2011 (2015).

64. Wang, J. *et al.* High performance Li-, Na-, and K-ion storage in electrically conducting coordination polymers. *Energy Environ Sci* **15**, 3923–3932 (2022).

65. Wang, J. *et al.* A High-Voltage Organic Framework for High-Performance Na- and K-Ion Batteries. *ACS Energy Lett* **7**, 668–674 (2022).

66. Markowski, R. Development of New Coordination Polymers for High-Performance Calcium Storage. (Université catholique de Louvain, 2022).

67. Dugas, R., Forero-Saboya, J. D. & Ponrouch, A. Methods and Protocols for Reliable Electrochemical Testing in Post-Li Batteries (Na, K, Mg, and Ca). *Chemistry of Materials* **31**, 8613–8628 (2019).

UNIVERSITÉ CATHOLIQUE DE LOUVAIN
Faculté des sciences
Place des sciences, 2 bte L6.06.01, 1348 Louvain-la-Neuve, Belgique | **www.uclouvain.be/sc**